Universal Journal of Civil Engineering
https://ojs.wiserpub.com/index.php/UJCE/

Research Article

Numerical Investigation of The Aerodynamics of Lorry Platooning Travelling through Road Tunnels

Xiaotian Zhang [1,2,3], David Soper [1], Bruño Fraga [1], Hassan Hemida [1,*] and Shidi Huang [2,3,*]

[1] School of Engineering, University of Birmingham, Birmingham, B15 2TT, Edgbaston, UK
[2] Department of Mechanics and Aerospace Engineering and Center for Complex Flows and Soft Matter Research, Southern University of Science and Technology, Shenzhen, 518055, Guangdong, China
[3] Guangdong Provincial Key Laboratory of Turbulence Research and Applications, Southern University of Science and Technology, Shenzhen, 518055, Guangdong, China
E-mail addresses: h.hemida@bham.ac.uk (H. Hemida) or huangsd@sustech.edu.cn (S.-D. Huang).

Received: 5 October 2022; **Revised:** 19 December 2022; **Accepted**: 30 December 2022

Abstract: With potential benefits in drag reduction and fuel saving, the aerodynamics of vehicle platoons have been investigated for a wide range of cases in open space. When vehicle platoons travel in road tunnels, the platooning strategy could be affected by the tunnel size, the traffic lane, and the inter-vehicle spacing. This paper presents a detailed investigation of these effects by numerically simulating the aerodynamics of an eight-lorry platoon travelling through road tunnels. The slipstream velocity and pressure fields, flow structures, and drag forces are examined as the inter-vehicle spacing are varied from 0.1L to 1.5L, where L is the length of a single lorry. It is found that the airflow induced by the moving platoon in the large tunnel (two-lane tunnel) is weaker than that in the small tunnel (single-lane tunnel), but similar to the case in the open air. As a result, the drag reduction due to platooning is most significant in the small tunnel, while the results in the large tunnel and the open air are largely identical. It is further found that, owing to the efficient shielding, the drag reduction in the open air increases monotonically as the inter-vehicle spacing decreases. However, the flow fields in both small and large tunnels change pronouncedly when the inter-vehicle spacing is 0.25L, resulting in relatively larger drag coefficients at this spacing. These findings are less sensitive to the traffic lane. This study provides useful insight into the platooning strategy of a long lorry platoon.

Keywords: Vehicle aerodynamics; Lorry platooning; Road tunnel; Drag reduction; Inter-vehicle spacing; Blockage ratio

1. Introduction

Vehicle platooning, whereby a series of vehicles travel in close proximity, is believed to be a promising solution to address modern traffic challenges, such as road congestion and fuel consumption. In recent years, the development of connected and autonomous vehicles through vehicle-to-vehicle communication has enabled platooning strategy to be considered in real scenarios. Therefore, this topic has received growing attention from both fundamental research and engineering applications.

It has long been known that platooning can lead to drag reduction, and this benefit has been utilized in many scenarios. Examples include bobsleigh crew members' position [1], cycling team racing [2, 3], marathon runners [4], and NASCAR (The National Association for Stock Car Auto Racing) [5]. These applications are believed to be inspired by the migrating geese, who fly in a V-shape platoon so that the flock can migrate over a great distance without rest [6]. To reveal the drag-reduction mechanism due to platooning, researchers have

DOI: https://doi.org/10.37256/ujce.2120231994

attempted some simple geometrical configurations, such as thin circular disks [7], cylindrical tubes [8–10], a rectangular plate placed downstream of an oval plate [11] and a flat disc followed by a cylinder [12]. It is found that there is an optimal inter-body spacing for the drag reduction, which allows the development of a quasi-steady vortex in the inter-body region, and thus the separating free shear layers of the leading body can re-attach onto the trailing body. As a result, the drag force reduces.

Similar behaviours in drag reduction associated with vehicles running in close proximity and the potential for fuel-saving have been identified by wind tunnel experiments [13–21] and fuel consumption track tests [22–27]. Research works based on computational fluid mechanics have provided detailed insights into the drag-reduction mechanism [24, 28–33]. These studies have illustrated that the drag reduction mainly results from the shielding effect. Briefly, the trailing vehicles are shielded from the high-speed airflow, therefore the drag force on the frontal surface is reduced. In addition, thanks to the trailing vehicles, the leading vehicle experiences an increased pressure in its rear region, and thus smaller pressure differential between the frontal and rear surfaces, which also contributes to the drag reduction.

To achieve greater fuel saving, researchers have also explored the optimal inter-vehicle spacing [15, 17, 18, 29, 34, 35]. The SARTRE (Safe Road Trains for the Environment) project, which aimed to develop a system that allows platoons to travel on public highways, showed that higher drag reduction and fuel saving could be achieved with smaller inter-vehicle spacing. Schito & Braghin [34] found that a 6-vehicle platoon with smaller inter-vehicle spacing has a smaller drag coefficient, and this finding is valid for a variety of vehicle geometries. In a recent experimental study of an eight-lorry platoon, Robertson et al. [15] also reported that the drag decreases as the inter-vehicle spacing decreases from 1.5L to 0.5L, where L is the length of a single vehicle. This study demonstrated that the shielding effect is more effective at smaller inter-vehicle spacing by reducing the frontal pressure.

However, some other studies have indicated that platooning does not always lead to dragging reduction for certain inter-vehicle spacings [13, 18, 26, 32, 33, 36–38]. Zabat et al. [18] first reported that the trailing vehicle experiences the most considerable drag reduction, but this effect reverses when the inter-vehicle spacing decreases below 0.2L. Pagliarella et al. and Watkins & Vino [36, 37] even reported a so-called “drag penalty” phenomenon for a two-vehicle platoon with small inter-vehicle spacing. Specifically, while the leading vehicle yields a significant drag reduction, the trailing vehicle experiences a higher drag than that in the isolation case. Le Good et al. [13, 19] also found a “drag penalty” for platoons consisting of 3-5 cars when the inter-vehicle spacing is 0.25L. A similar phenomenon was observed by Mirzaei & Krajnović [33], who used Large-Eddy Simulation to investigate a two-Ahmed-body platoon, and indicated a “drag penalty” for two inter-vehicle spacings (0.3L and 0.5L). Recently, Ebrahim & Dominy [32] investigated the performance of a car platoon with inter-vehicle spacing ranging from 0L to 1.0L. This study found that, for the inter-vehicle spacing of 0.25L and 0.5L, the impinging flow will cause the drag to exceed the vehicle-in-isolation case. Törnell, Sebben, & Elofsson [21, 39] reported that the drag of the trailing truck in a two-vehicle platoon increased as the inter-vehicle spacing dropped down from 20 meters to 5 meters, after which the drag decreased as the spacing decreased. These studies suggest that the drag properties associated with vehicle platooning are sensitive to the vehicle geometry and the inter-vehicle spacing. Moreover, McAuliffe & Ahmadi-Baloutaki [20] noted that it is important to take real road conditions into account; otherwise, the advantage of platooning could be overstated. Therefore, more detailed studies are required to understand the effects of inter-vehicle spacing on different types of vehicle platoons that are likely to occur in real scenarios.

One important scenario that should be considered is when vehicles travel in road tunnels. The tunnel walls will not only restrict the airflow motion but also modify the aerodynamics of the vehicles via the so-called piston effect. Specifically, unlike the case of vehicles traveling in the open space, where the air displaced by the vehicles can freely move away to most directions, the airflow around vehicles in a tunnel is mostly pushed to proceed in the same direction as the vehicles. As a result, a high-pressure region is formed in the front of the vehicle and a low-pressure region behind it, where the wake structures act as an air-sucker. These changes in the flow field lead to significant variations in the aerodynamic forces. Therefore, investigating the aerodynamics of vehicles travelling through road tunnels is critical for optimising the platooning strategy.

Previous research on this topic primarily focused on the time-averaged quantities (such as airflow velocity and forces coefficient), and their dependences on the vehicle velocity and the traffic density (or the inter-vehicle spacing). By using model-scale experiments, Chen et al. [40] found that the vehicle speed had a greater influence on the piston effect than the inter-vehicle spacing and the vehicle size. Sambolek [41] reported that the time-averaged airflow velocity in the tunnel decreases as the vehicle speed increases. Katolický & Jícha [42] also reported that the airflow in the tunnel depends on the vehicle speed, as well as the traffic density. However, the airflow induced by the vehicles eventually approaches a saturated value at a certain traffic density. Recently, Lee et al. [43] investigated the drag coefficients of sedans in a double-deck tunnel. The influences of the

blockage ratio (the cross-section area of the vehicle over that of the tunnel), the vehicle speed, and the inter-vehicle spacing were evaluated. This study showed that the time-averaged drag coefficient increases with an increase in the blockage ratio and the inter-vehicle spacing, but with a decrease in the vehicle speed. In addition, a negative interaction was observed between the vehicle speed and the inter-vehicle spacing. However, most of these studies were conducted under stable or quasi-static conditions, which are different from the actual airflows in road tunnels.

With the development of modern experimental technology and computational ability, more studies have begun to investigate moving vehicles in road tunnels with the transient aerodynamics being accounted for. Different approaches have been used to model the relative movement between the vehicles and the tunnel, such as using a porous jump-moving wall [44], adopting a relative velocity [45], and employing the dynamic mesh technique [46–48]. In the numerical studies of a two-vehicle platoon travelling in a curved tunnel, where the inter-vehicle spacing was varied from 1.5L to 10L, F. Wang et al. [46, 47] found that even if the inter-vehicle spacing is large, the drag coefficients of the vehicles in platooning are lower than that of a single vehicle. In addition, the drag coefficient decreases with decreasing the inter-vehicle spacing but slightly increases as the vehicles slow down. However, in a reduced-scale tunnel experiment, Sike et al. [49] found that the influence of the vehicle speed is more significant than the inter-vehicle spacing. Bhautmage & Gokhale [45] found that vehicles travelling at high speed with smaller inter-vehicle spacing produce larger wake structures, but the corresponding drag coefficients were not examined.

To gain a better understanding of the aerodynamics associated with vehicle platooning running in road tunnels, a recent study investigated the case of an eight-lorry platoon using both model-scale experiments and numerical simulations [50]. The most interesting finding of that study is that the drag reduction effect due to platooning is larger in the tunnel than that in the open air. However, owing to the limitation of the laboratory conditions, the experiments and thus the corresponding numerical simulations in that study were performed in a single-traffic-lane tunnel with a blockage ratio being 36%. Since the blockage ratio has a significant effect on the drag coefficient [43], it is worth checking whether the above-mentioned interesting finding is valid in a large tunnel with a smaller blockage ratio. In addition, as the majority of road tunnels have multiple traffic lanes, the effect of the traffic lane is also of interest. Moreover, previous studies of vehicles travelling in road tunnels mainly explored cases with large inter-vehicle spacings. It is not clear whether the “drag penalty” phenomenon, which was observed for platoons with small inter-vehicle spacing in the open air, also exists in road tunnels.

Following the motivations above, this paper reports a numerical investigation of the effects of blockage ratio (BR), traffic lane, and inter-vehicle spacing on the aerodynamics of lorry platooning, with a focus on the drag properties. Lorry platoons running under four different circumstances are investigated: in the open air, in a small tunnel (BR =36%, similar to single-lane tunnels), in a large tunnel (BR =15%, similar to two-lane tunnels), and along the right traffic lane of the large tunnel. The inter-vehicle spacing is varied from 0.1L to 1.5L, where L is the length of a single lorry. A Detached Eddy Simulation methodology is employed in the present study, which is introduced in Section 2. After showing the validation of the numerical model in Section 3, a detailed analysis of the flow fields and the drag properties are presented in Section 4. The effects of the blockage ratio and the traffic lane are first discussed in Section 4.1, and then the effects of the inter-vehicle spacing are in Section 4.2. Finally, the major findings are highlighted in Section 5.

2. Computational models and methods

2.1 *Description of the vehicle and the platoon*

In this study, a 1/20th scale box-type lorry (see Figure 1) was used. It has a dimension of 0.395 m, 0.175 m, and 0.125 m for length (L), height (H), and width (W), respectively. This lorry model is simplified from a commercial Leyland DAF 45-130 vehicle, which has been extensively investigated in previous studies [15, 28, 50–54]. Despite some simplifications, such as the removal of side mirrors and windshield overhangs, these simplifications do not significantly affect the aerodynamic performance of the lorry model but help to reduce the numerical efforts greatly [52, 55, 56].

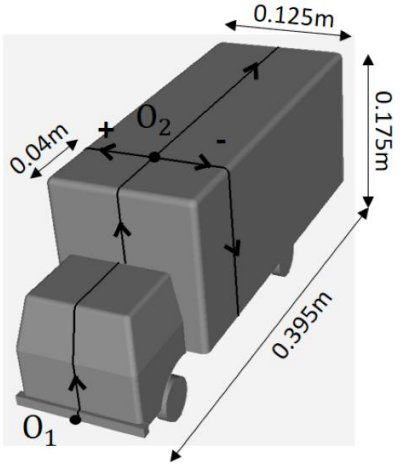

Figure 1. The shape and dimensions of the model-scale lorry used in the experiments. The two black solid lines with arrows on the lorry's surface indicate the positions for the surface pressure analysis, which will be presented in Section 4.2.2

The platoon of the present study consists of eight lorries. It has been proven in previous studies [15, 28, 50, 54] that an eight-vehicle platoon is long enough to ensure boundary layer development so that the aerodynamics of the platoon can be fully examined. The platoon travels at a nominal speed $V_{plat} = 25$ m/s, which yields a Reynolds (Re) number of 3×10^5 based on the height H of the lorry. Although this Re number is lower than the full-scale value, it is high enough for the examination of aerodynamic coefficients [57]. Previous model-scale experiments and numerical simulations for bluff vehicles conducted at Re numbers of $\sim 10^5$ have shown good agreement with full-scale data [52, 58, 59].

2.2 *Simulation methodology and numerical schemes*

Airflow around a bluff body is highly turbulent. Because of the higher accuracy in reproducing unsteady flow characteristics, Large Eddy Simulation (LES) provides an efficient solution to this problem. However, LES requires vast computational resources, especially for high Re number flow [60]. On the other hand, Reynolds Averaged Navier-Stokes (RANS) is more widely used to simulate vehicle aerodynamics [46, 61–64], because it has a lower requirement for mesh density than LES. The present study adopts Improved Delayed Detached Eddy Simulations (IDDES). The principle of IDDES is that the attached flow near the wall is simulated with RANS, while the detached flow is resolved with LES. As a result, the mesh density is largely reduced for IDDES, so this method is a more flexible approach for simulating high Re number flow. It has been demonstrated by Niu et al. [65] that using IDDES based on the Shear Stress Transport (SST) k–ω model can better simulate turbulent flow involving boundary layers with adverse pressure gradients, separation, and recirculation. Details about the SST-IDDES model can be found in [66, 67].

The simulations are performed using commercial software (ANSYS Fluent 18.2) based on a pressure solver with the finite volume method. For the pressure and velocity coupling equations, the SIMPLE (Semi-Implicit Method for Pressure-Linked Equations) algorithm is applied. The bounded central differencing scheme is used to solve the momentum equations. The second-order upwind scheme is applied to solve the k and ω transport equations. The time advancement is conducted using a second-order implicit scheme, and the time step is set to be 1×10^{-4} s [50,68,69]. Note that a smaller time step (0.5×10^{-4} s) has also been tested in this work to confirm that the present time step is sufficient. The number of iterations is set to be 50 for each time step so that the residual is sufficiently small before considering the solution converged.

2.3 *Computational domain and boundary conditions*

The computational domain is illustrated in Figure 2. It consists of stationary and moving sub-domains. The origin of the coordinate system is at the tunnel's portal and centre of the roadway on the tunnel floor, with the x-axis being positive in the platoon's travelling direction, and the z-axis pointing vertically upward. The width and height of the stationary domain are 40.14H and 20.6H, respectively. The sliding mesh technique is adopted to simulate the relative movement between the lorry platoon, the ground plane, and the tunnel. This technique has been used to simulate vehicles travelling in a tunnel [50, 70–72]. More detailed information about this technique can be found in Chu et al. [73]. According to the best practice guidelines [71, 74], the simulation results must be

amended when the ratio of the tunnel's cross-section to the computational domain is between 5% and 15%. In the present study, this area ratio is 2%, so the results do not need to be amended.

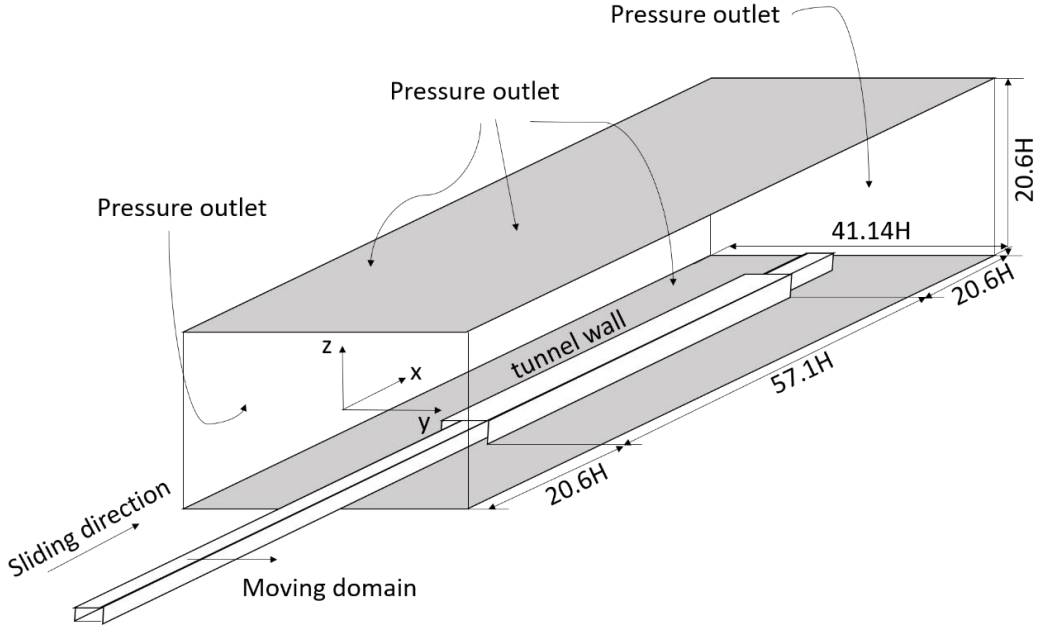

Figure 2. The dimensions and the boundary conditions of the computational domain.

The boundary conditions for the computational domain are also shown in Figure 2. The top, side, front and back faces of the computational domain are defined as the pressure outlet boundaries and the reference pressure was set to zero. The no-slip wall boundary conditions are specified for the lorry surfaces, the ground plane, and the tunnel walls. To ensure that the turbulent flow around the platoon is fully developed, the simulations start when the leading lorry is 20.6H away from the tunnel's portal and stop when the last lorry is also 20.6H away from the tunnel's exit. Note that the present study adopted the sliding mesh technique to simulate the relative movement between the lorry platoon, the ground plane, and the tunnel, which is different from the usual stationary simulations. In other words, the platoon is moving in the simulations and the airflow is induced by the movement of the platoon. Therefore, the velocity inlet boundary condition is not required in the present study. Only the speed of the platoon ($V_{plat} = 25$ m/s) should be specified in the simulations.

2.4 *Simulation cases*

To investigate the effects of blockage ratio, traffic lane, and inter-vehicle spacing, a series of simulations are conducted in the present study. To be specific, platoons travelling under four different circumstances (see Figure 3) are simulated: in the open air (OA), in a large tunnel (LT), along the right traffic lane of the large tunnel (RLT), and in a small tunnel (ST). The OA cases are simulated as references. The ST cases are identical to the tunnel experiments that have been investigated previously with a fixed inter-vehicle spacing of 1.5L [50], in which the effect of the inter-vehicle spacing remains to be explored. The LT cases are used to determine the influence of the blockage ratio, and the RLT cases are used to examine the effect of the traffic lane. Note that the blockage ratio of the large tunnel (15%) is similar to the cases of real road tunnels with two traffic lanes. For the effects of the inter-vehicle spacing, platoons with six different cases are investigated (see Figure 4).

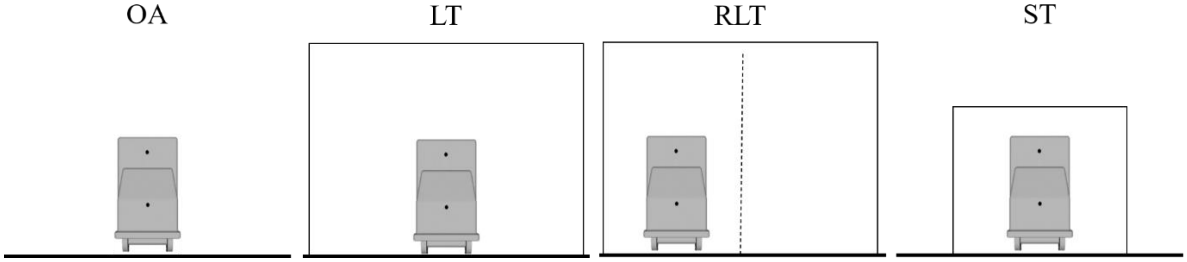

Figure 3. Platoons travel under different circumstances. OA: in the open air; LT: in a large tunnel; RLT: along the right traffic lane of the large tunnel; ST: in a small tunnel.

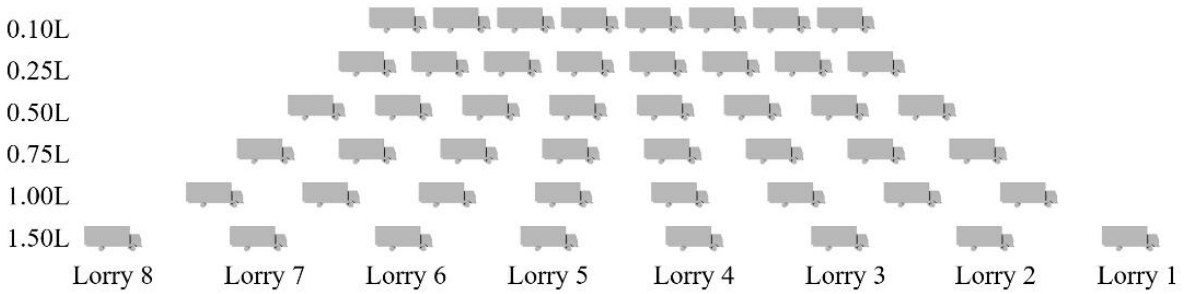

Figure 4. Platoons with different inter-vehicle spacings ranging from 0.1L to 1.5L.

3. Mesh independence and numerical validation

The quality of the IDDES model depends on the mesh resolution because the blending process between the RANS and LES is affected by the cell size [75]. The surface grid for the lorry is shown in Figure 5(a, b). Meshes for a horizontal slice of the entire domain are displayed in Figure 5(c). The meshes in the present work are structured hexahedral grids generated by the commercial software Ansys ICEM-CFD. Sufficient refinement close to the solid walls is made to resolve the critical flow features. Three sets of meshes (shown in Table 1) are used to verify the independence of the meshes.

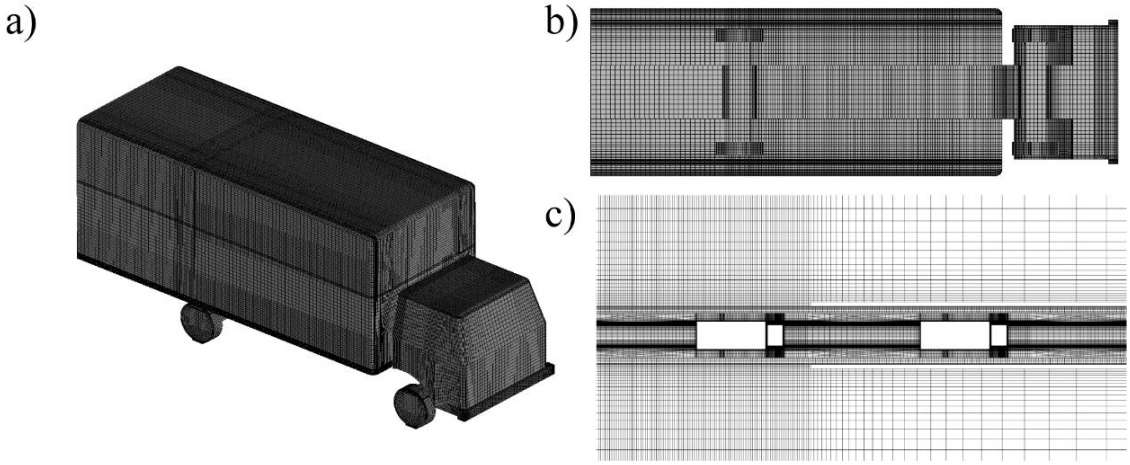

Figure 5. Computational grid used in the present study: (a) mesh for the surfaces of the lorry's cab and box; (b) mesh for the lorry's bottom surface; (c) mesh for a horizontal plane of the whole domain at $z/H = 0.57$.

Table 1. The parameters for the grid sensitivity test in the present study

	Coarse	Medium	Fine
Averaged y^+	5	2	1
Number of mesh cells in the moving domain (million)	20.3	28.2	35.5
Number of mesh cells in the stationary domain (million)	10.5	14.6	14.6
Total number of mesh cells (million)	30.8	42.8	50.1

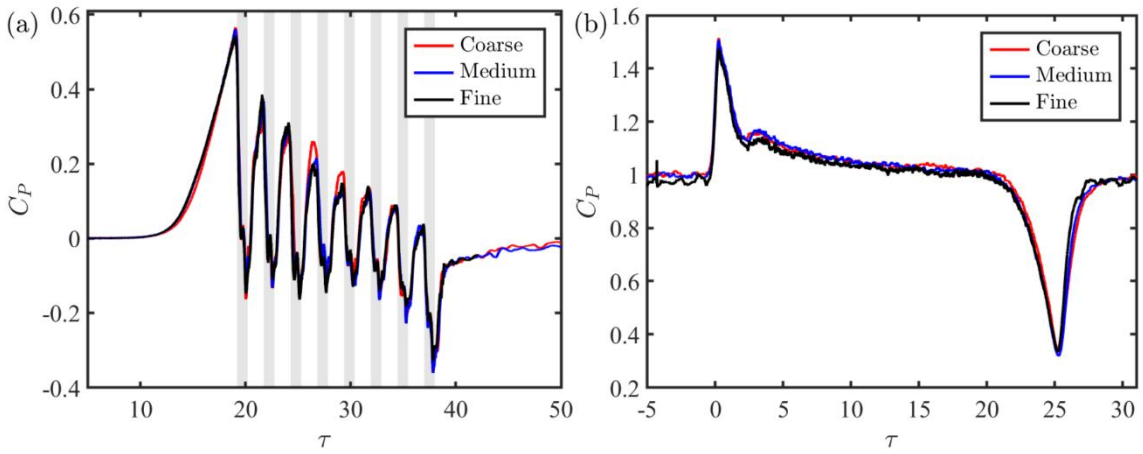

Figure 6. Pressure coefficients for different mesh densities: (a) slipstream pressure at 40H away from the tunnel's entrance, 0.45H above the ground plane, and 0.14H away from the lorry body; (b) surface pressure on the cab's centre of the leading lorry. The shaded rectangles in (a) indicate the time for each lorry in the platoon passing through the monitoring point.

Figure 6 shows the pressure coefficients in the tunnel and the surface pressure coefficients on the cab centre of the leading lorry obtained from the simulations using different numbers of cells. The pressure coefficient C_p is defined below:

$$C_p(\tau) = \frac{p(\tau) - p_\infty}{\frac{1}{2}\rho_\infty V_{plat}^2} \tag{1}$$

Here, the normalized time $\tau = V_{plat}t/L$ is set to zero when the leading lorry enters the tunnel. p_∞ and ρ_∞ are the pressure and the density of the room air in the experiments. It is seen that the results for the medium and fine meshes compare well with each other. In addition, the IDDES method recommends that $y^+ \sim 1$ for the mesh resolution [67]. Therefore, the fine mesh is adopted in the present study.

The quality of the mesh has been checked by the Courant-Friedrichs-Lewy number (CFL $= V_{plat}\Delta t/\Delta x$, where Δx represents the cell length and Δt is the time step). It is found that the CFL number remains below one, with only a small number of localized exceptions occurring. Previous studies have shown that this minor infringement on the stringent CFL requirement has no significant effect on the simulations [76–78]. The quality of the mesh has been checked by other quantities as well, such as the blending function and the turbulent viscosity ratio, which also confirm that the present mesh meets the requirement of the IDDES model [39].

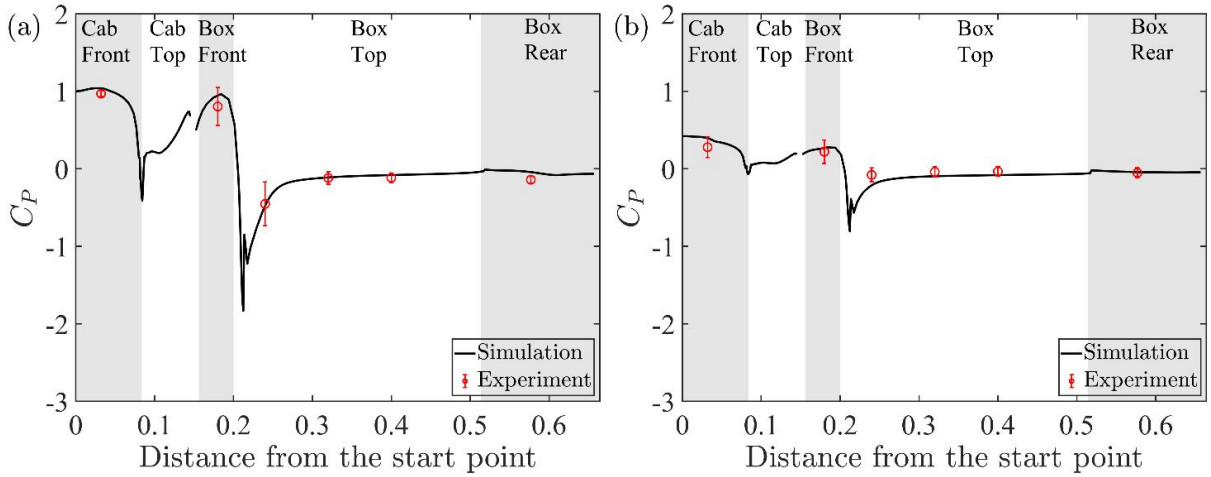

Figure 7. The time-averaged surface pressure coefficients of different lorries along the central line (see the solid line O1 in Figure 1) of the platoon in a small tunnel: (a) Lorry 1; (b) Lorry 5. The shaded areas are used to distinguish different regions along the lorry's surface.

The numerical model has been validated by comparing it with experimental results (including slipstream properties, surface pressures, and drag coefficients) obtained by Zhang et al. [50] and Zhang [79]. For example, Figure 7 shows the surface pressure distribution of different lorries along the central line. It is seen that the numerical data are in good agreement with the experimental ones, demonstrating the reliability of the numerical model. More details about the numerical validation can be found in Zhang et al. [50] and Zhang [79].

4. Results and Discussion

4.1 *Effects of blockage ratio and traffic lane*

In this section, the effects of blockage ratio and traffic lane on the slipstream properties, flow structures, and aerodynamic forces are investigated. The inter-vehicle spacing of the platoon is fixed at 1.5L, which can reflect typical road conditions appropriately. Smaller inter-vehicle spacings are more relevant to connected and autonomous vehicle technologies and will be discussed in the following section.

4.1.1 *Flow field analysis*

Figure 8 shows the instantaneous velocity fields at a horizontal plane of $z/H = 0.57$ for lorry platoons running under different circumstances. Here, the non-dimensional horizontal velocity is defined as:

$$U_{res}(\tau) = \sqrt{(\frac{u(\tau)}{V_{plat}})^2 + (\frac{v(\tau)}{V_{plat}})^2}, \quad (2)$$

where u and v represent the longitudinal and lateral velocity components, respectively. This dimensionless velocity includes both the streamwise and spanwise velocities of the airflow induced by the moving platoon, so it provides a more accurate assessment of the slipstream velocity and its effects on passengers [15]. The influence of the blockage ratio on the aerodynamic flow is reflected by the velocity magnitude, which indicates that the moving platoon in the small tunnel induces a stronger piston effect than those in the large tunnels. However, in terms of the velocity distribution pattern, the airflows created by the platoons in the large tunnels are similar to that in the open air, and the difference between the LT and RLT cases is not obvious in this figure.

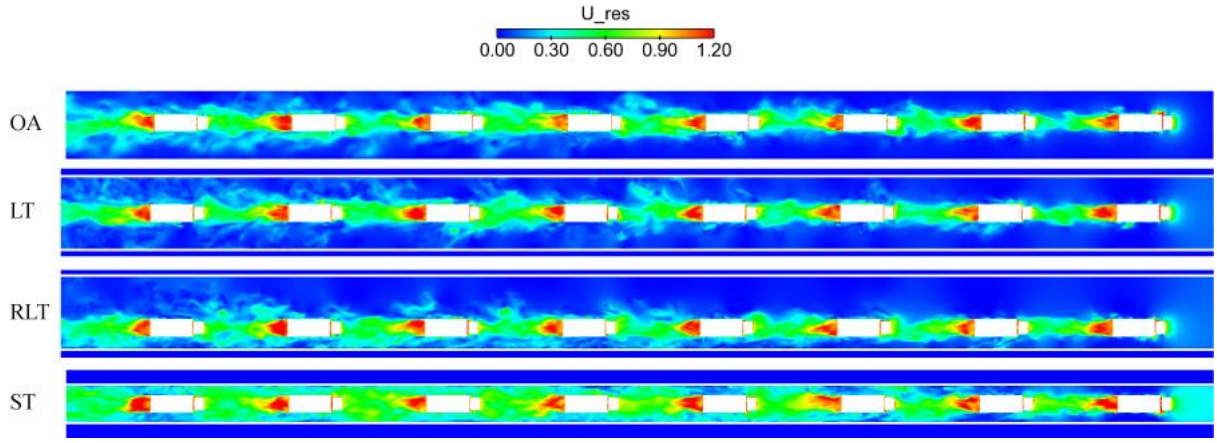

Figure 8. Instantaneous velocity fields at the horizontal plane of $z/H = 0.57$ for lorry platoons running under different circumstances. The velocity magnitude is coded by the colour.

It is further observed in Figure 8 that the largest velocity magnitude occurs in the rear wake region of each lorry for all the cases examined. To better visualize the flow structures in this region, Figure 9 shows time-averaged streamlines at the centreline plane for three representative lorries in the platoons running under different circumstances. Each lorry serves as a static reference for the generation of streamlines, which are averaged over the period of $\tau = 7.5{\sim}17.5$ when the lorries are travelling inside the tunnel. As the overall features of the flow fields around intermediate lorries in the platoons are similar, the fifth lorry is taken as the representative of intermediate lorries for analysis. It is seen that, compared with the cases in the open air, the upper vortices in the rear region are enlarged for all the lorries in the small tunnel. While in the large tunnel, the vortices behind the first and fifth lorries are similar to those in the open air, but the vortices behind the last lorry are similar to those in the small tunnel. When the platoon is running along the right lane of the large tunnel, the vortex structures are similar to those in the LT case.

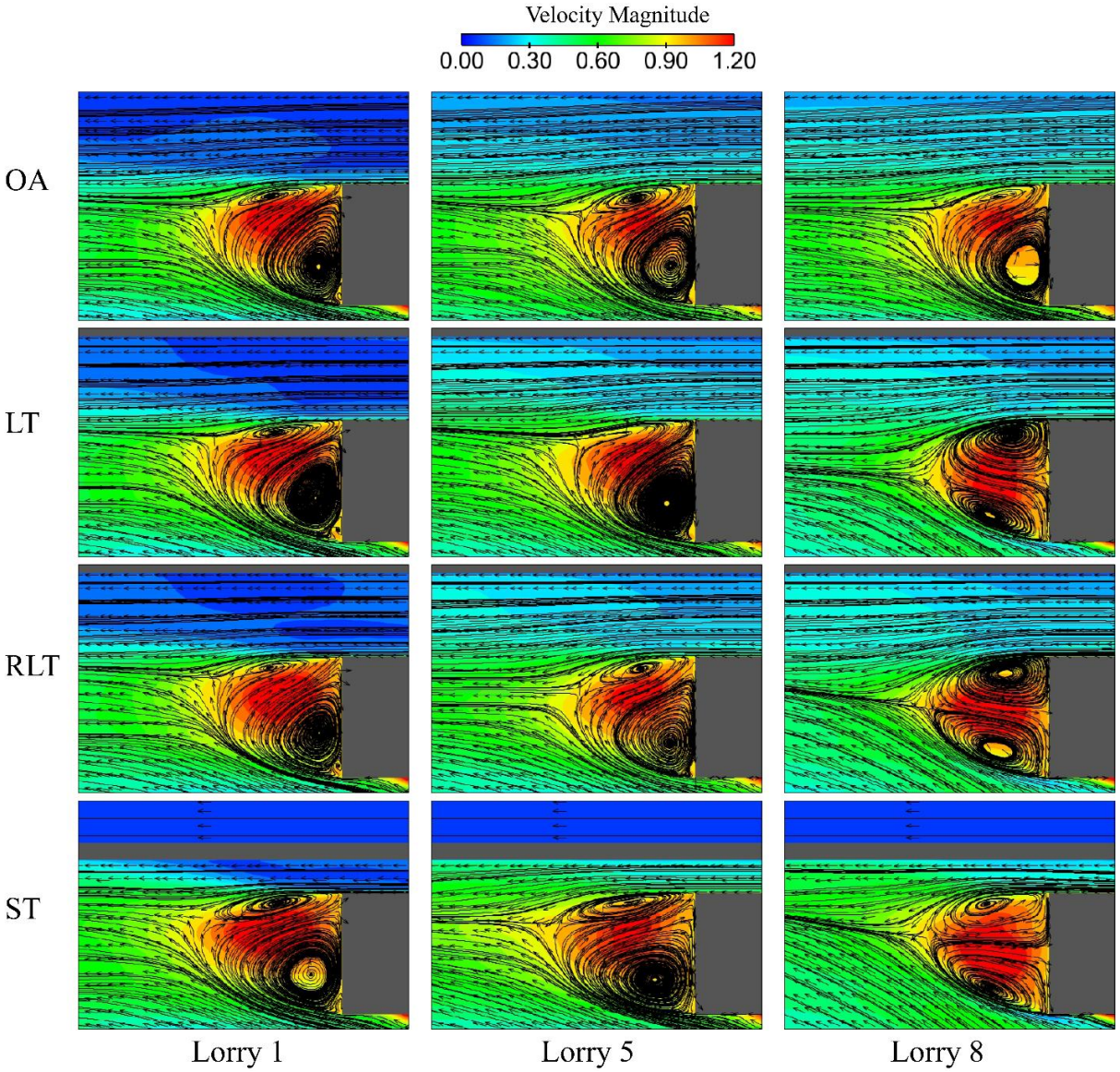

Figure 9. Time-averaged velocity fields in the rear region of three representative lorries in the platoons running under different circumstances. The data are obtained at the centreline plane of $y/H = 0$. The solid lines are streamlines and the arrows represent velocity vectors. The velocity magnitude is coded by the colour.

To reveal the effects of the traffic lane, Figure 10 shows the time-averaged streamlines (over the time of $\tau = 7.5 \sim 17.5$) at the $z/H = 0.57$ plane for three representative lorries in the platoons running in the large tunnel. It is seen that the wake structures become asymmetric when the platoon is running along the right lane, which is more obvious for the last lorry. Furthermore, as indicated by the coding colour, the flow strength increases between the lorries and the side closer to the tunnel wall but remains relatively unaffected on the more open side. This could be understood as the effect of local blockage due to the tunnel wall.

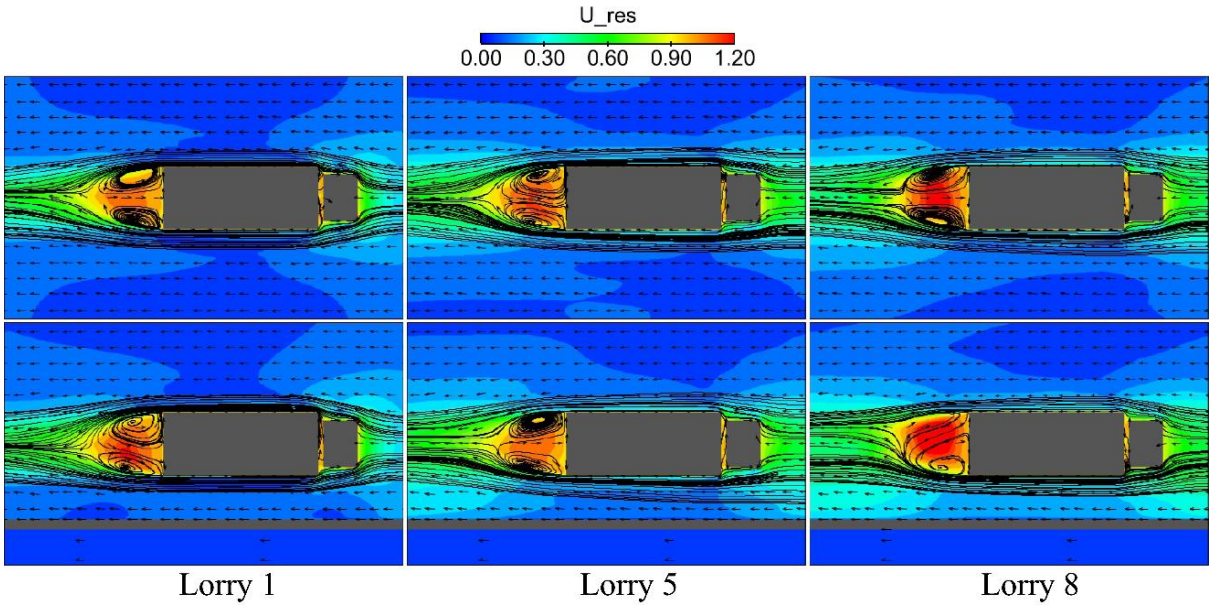

Figure 10. Top view of time-averaged velocity fields around three representative lorries in the platoon at the plane of $z/H = 0.57$. Top panel: in the large tunnel. Bottom panel: along the right lane of the large tunnel. The solid lines are streamlines and the arrows represent velocity vectors. The velocity magnitude is coded by the colour.

The blockage ratio also has a strong impact on the pressure field. It is seen in Figure 11 that, the frontal positive pressure is largest for the platoon in the small tunnel, then the two cases in the large tunnel, and finally the case in the open air. It is further seen that the frontal pressures progressively drop from the leading lorry to the last one for all the cases, which is more significant in the small tunnel. Moreover, the positive pressure in the frontal region of the first few lorries and the negative pressure in the rear region of the last lorry is also more pronounced in the small tunnel. This piston-induced effect is less so for the two cases in the large tunnel, which depends weakly on the traffic lane. A closer look at Figure 11 reveals that the pressure fields ahead of the first few lorries for the RLT case become stronger and asymmetric on the side closer to the tunnel wall. As will be shown in the next section, these differences in the velocity and pressure fields result in different drag forces for the lorries in the small and large tunnels.

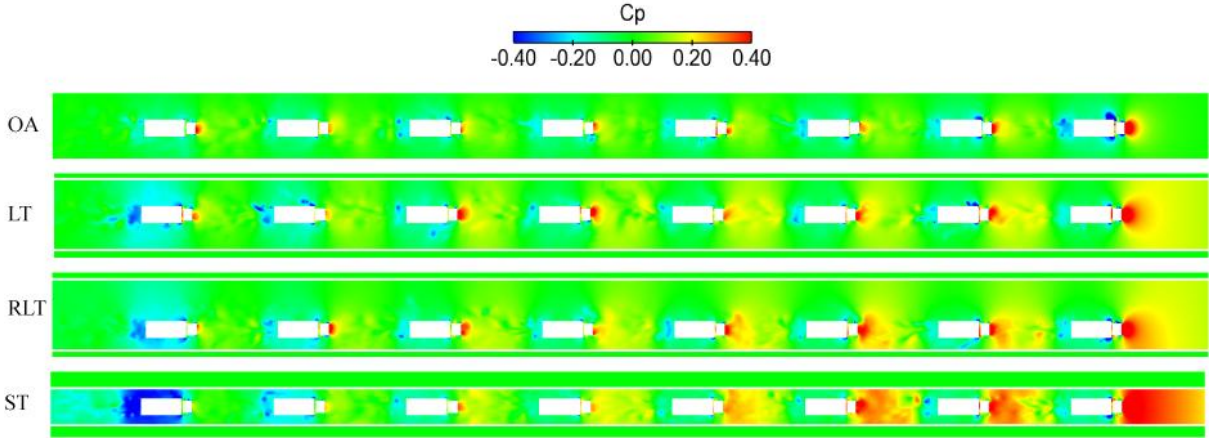

Figure 11. Instantaneous pressure fields at the horizontal plane of $z/H = 0.57$ for the platoons running under different circumstances. The pressure magnitude is coded by the colour.

4.1.2 *Aerodynamics force analysis*

Two types of aerodynamic forces are examined in this section, i.e., the drag force F_f and the side force F_s. The non-dimensional force coefficients are defined as:

$$C_d = \frac{F_f}{0.5\rho V_{plat}^2 A_f}, \tag{3}$$

$$C_s = \frac{F_s}{0.5\rho V_{plat}^2 A_f} .$$

Here, A_f is the referenced surface area, which has been taken to the cross-section of the lorry normal to the x-axis.

Table 2. The coefficients of drag force and side force for a single lorry running under different circumstances and the corresponding root mean square (r.m.s.) values

	$C_{d-single}$	r.m.s.	$C_{s-single}$	r.m.s.
Open air (OA)	0.62	0.02	0.0035	0.0386
Large tunnel (LT)	0.71	0.02	0.0027	0.0419
Right lane of large tunnel (RLT)	0.74	0.03	0.0072	0.0417
Small tunnel (ST)	0.96	0.03	0.0026	0.0461

First of all, the force coefficients of a single lorry are determined as the baseline (Table 2). Note that the data are averaged over the time of $\tau = 7.5{\sim}17.5$ when the lorry is running through the middle section of the tunnel. For the data in the open air, the corresponding time-averaging is made. As seen in Table 2, the drag coefficient of a single lorry increases from 0.62 in the open air to 0.96 in the small tunnel, indicating a considerable impact on the blockage ratio. However, the drag coefficients for the LT and RLT cases are approximately the same within the uncertainty (indicated by the r.m.s. values). In terms of the side force, although the data for the RLT case is about 3 times larger than that in the LT case, possibly owing to the asymmetric flow field, the values are too small to induce lateral instability. The time-averaged values of side forces are even much smaller than the r.m.s. values (see Table 2), suggesting that side force is not important for a single lorry.

Figure 12 illustrates the temporal variation of drag coefficients for all lorries in the platoons running under different circumstances. Here, $\tau = 0$ indicates the time when each lorry enters the tunnel and $\tau = 25$ represents the time leaving it. It is seen that the trailing lorries for all the cases benefit from the shielding effect due to platooning, with the most significant drag reduction occurring between the leading lorry and the second one. In the small tunnel, the drag coefficients of all lorries increase dramatically when entering the tunnel, then gradually fall as travelling through the tunnel before abruptly decreasing at the exit. For the data in the large tunnel, such variations are less pronounced. In addition, while the drag coefficients for most of the trailing lorries in the small tunnel are visibly different, the data for trailing lorries in the large tunnel have roughly the same magnitude, which is similar to the case in the open air.

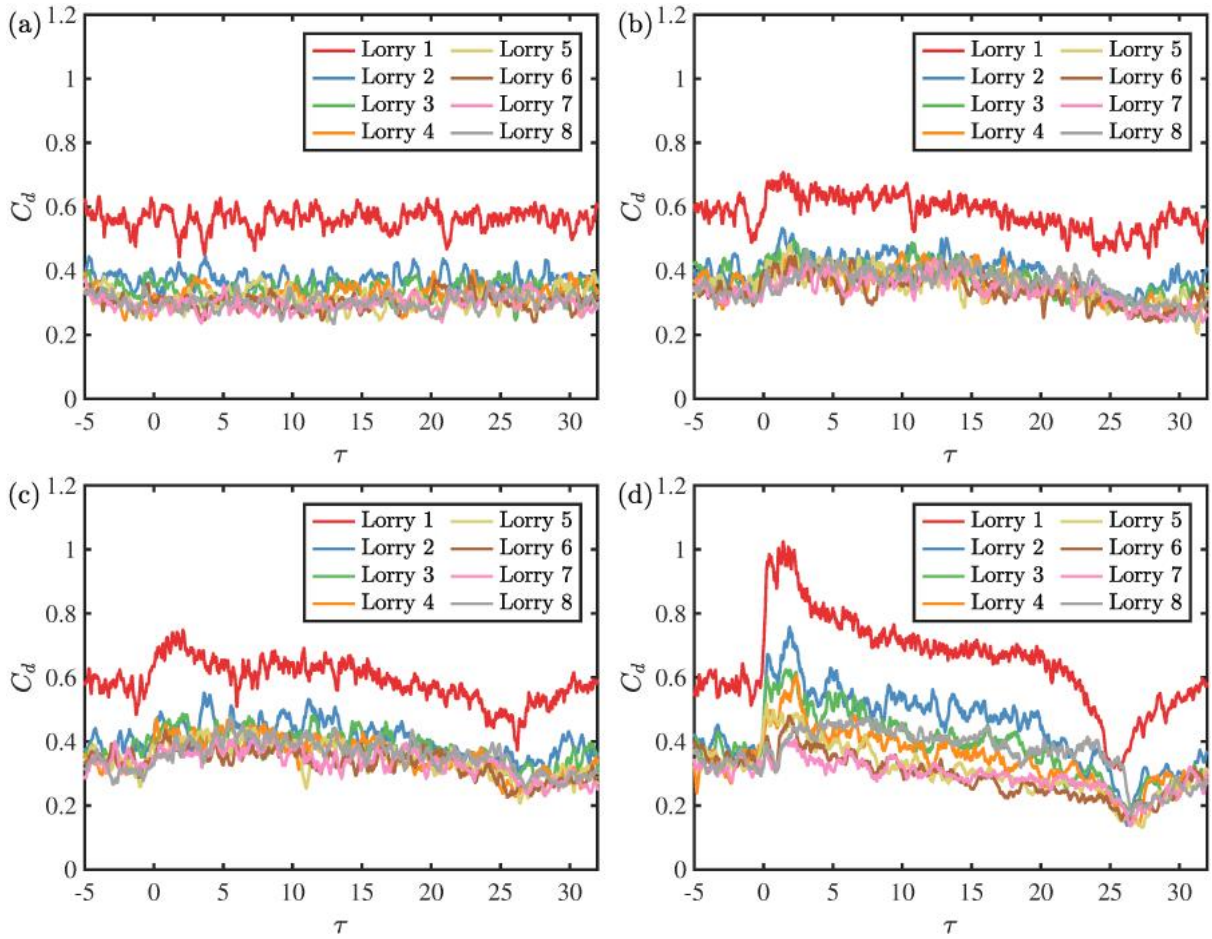

Figure 12. Temporal variation of drag coefficients for all lorries in the platoons running under different circumstances: (a) in the open air, (b) in the large tunnel, (c) along the right lane of the large tunnel, and (d) in the small tunnel.

To make a direct comparison, the data in Figure 12 are averaged over the time of $\tau = 7.5{\sim}17.5$ and then plotted in Figure 13(a). The differences between the drag coefficients in the open air and the small tunnel have been reported in a previous study [50]. There is a sudden increase in the drag coefficient of the last lorry in the small tunnel, owing to the strong negative pressure in the rear region. Drag coefficients in the large tunnel exhibit almost independence of the traffic lane, with the magnitudes being consistently larger than those in the open air. When compared with the small tunnel, the drag coefficients in the large tunnel are smaller for the first two lorries, thanks to a weaker piston effect. However, the data become larger for the fourth to the seventh lorries. This is because the frontal pressures for these lorries diminish slower than those in the small tunnel, as shown in Figure 11. Figure 13 also reveals some effects of the vehicle number. When the vehicle number exceeds five, the drag coefficients for the intermediate lorries trend to level off. This suggests that a platoon consisting of five vehicles could be long enough for studying the aerodynamics of the platoon. For a shorter platoon, because the boundary layer around the platoon is not fully developed [15], the drag properties would behave differently. Detailed effects of the vehicle number are subject to future study.

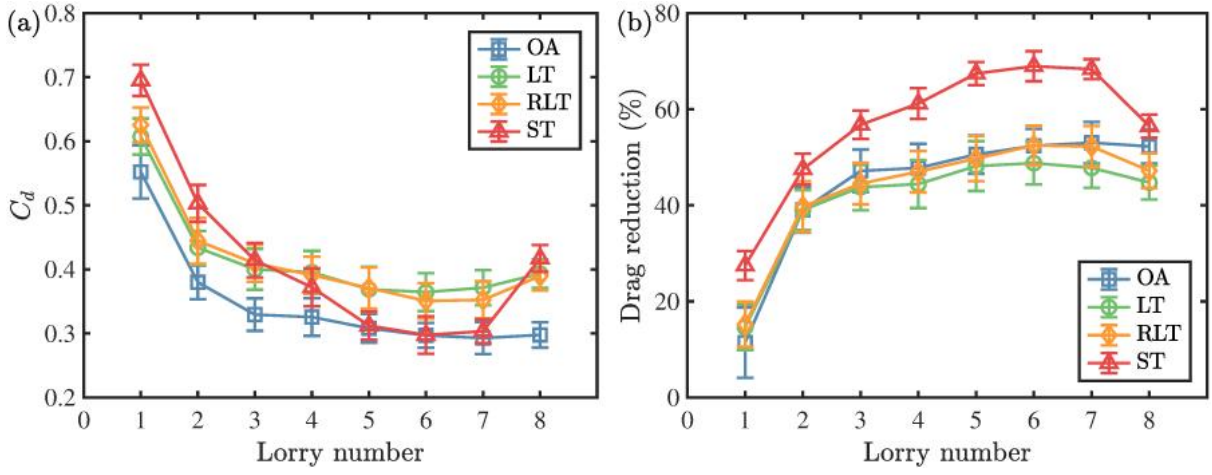

Figure 13. A comparison of (a) time-averaged drag coefficients and (b) drag reduction ratio in terms of $(1-C_d/C_{d-single})\times 100\%$ for all lorries in the platoons under different circumstances.

Because the drag coefficients of a single lorry are different for different circumstances, it is more meaningful to compare the drag reduction ratio in terms of $(1-C_d/C_{d-single})\times 100\%$. It is seen in Figure 13(b) that, because of the strong piston effect, the drag reduction is most significant in the small tunnel. Interestingly, although the drag coefficients in the large tunnel are larger than those in the open air, their drag reduction ratios are almost identical. It is not clear whether this phenomenon is valid for other blockage ratios (i.e., tunnel sizes). At this stage, we believe it could be coincidental. If taking the results in the small tunnel into account together, one would expect that the drag reduction ratio could have other different values for different blockage ratios. Thus, to have a clear understanding of this phenomenon, more blockage ratios should be explored.

Finally, the coefficients of side force are examined to check whether the lorries in platooning would experience any lateral instability. From Figure 14, it is seen that the time-averaged coefficients of side force (over the time of $\tau = 7.5\sim17.5$) are considerably small for all the cases, which are even smaller than the r.m.s. values (order of ± 0.05). A similar level of r.m.s. values have been found for lorry platoons with different inter-vehicle spacings, so the effect of side force is not important here. The following section will not discuss the side force anymore.

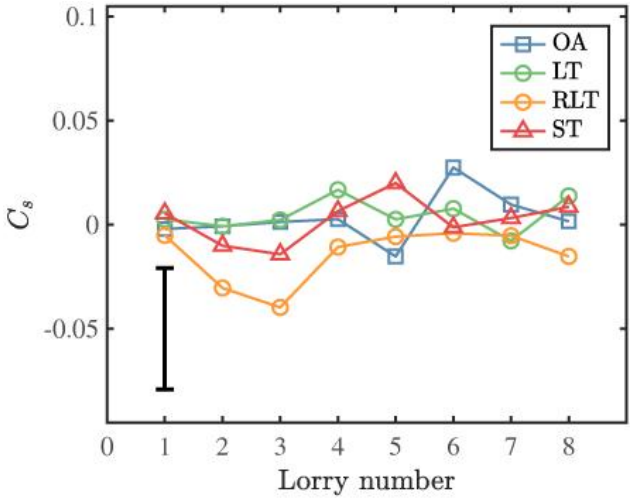

Figure 14. Time-averaged coefficients of side force for all lorries in the platoons under different circumstances. The error bar in the left corner is averaged over the r.m.s. values of all the cases.

4.2 *Effects of inter-vehicle spacing*

In this section, the effects of inter-vehicle spacing will be discussed. Six different cases as illustrated in Figure 5 are examined. For the sake of simplicity, only four typical spacings (0.1L, 0.25L, 0.5L, and 1.0L) will be exhibited in the flow field analysis.

4.2.1 *Flow field analysis*

Figure 15 shows the transient pressure fields around the platoons with different inter-vehicle spacings and under different circumstances. Similar to the results shown in Figure 11, the airflow created by the moving platoons is most significant in the small tunnel, but less so in the large tunnel. The asymmetric pressure patterns are also obvious for all the RLT cases. In addition, the key features of the positive pressure ahead of the first lorry and the negative pressure behind the last lorry are similar for the platoons with different inter-vehicle spacings. However, the pressure variation trend is different for the intermediate lorries.

To show the different behaviour more clearly, Figure 16 presents the time-averaged pressure fields (over the period of $\tau = 7.5\sim17.5$) around the fifth lorry as a representative example. It is seen that the frontal pressures decrease monotonically as the inter-vehicle spacing decreases for all the cases, but the rear pressures in the tunnels are substantially larger at 0.25L than other inter-vehicle spacings, in contrast to the data in the open air. This suggests that the drag coefficients may behave differently for the platoons with 0.25L spacing in the tunnels.

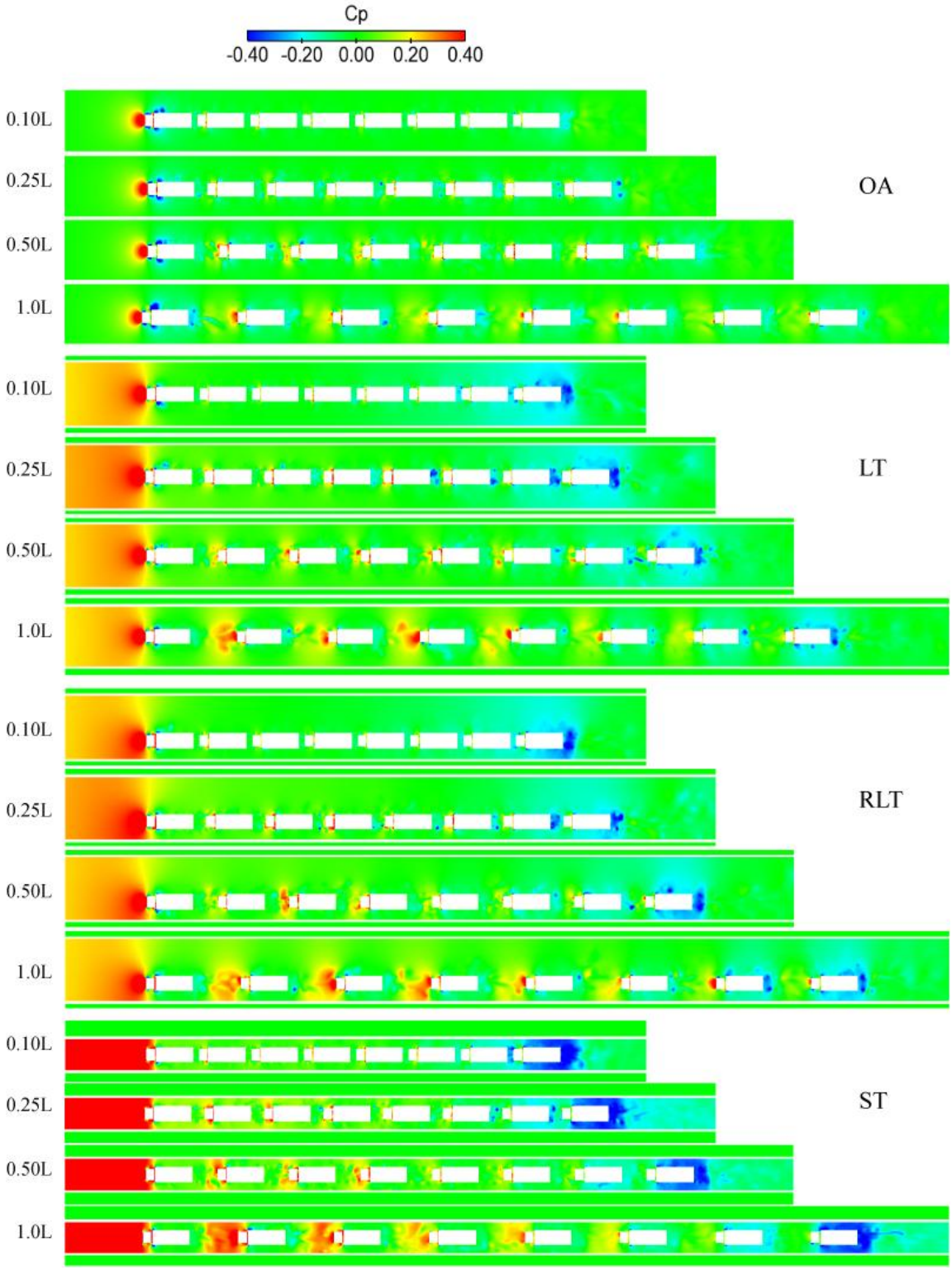

Figure 15. Instantaneous pressure coefficient fields for lorry platoons with different inter-vehicle spacings and running under different circumstances. The data are obtained at the horizontal plane of $z/H = 0.57$. The pressure magnitude is coded by the colour.

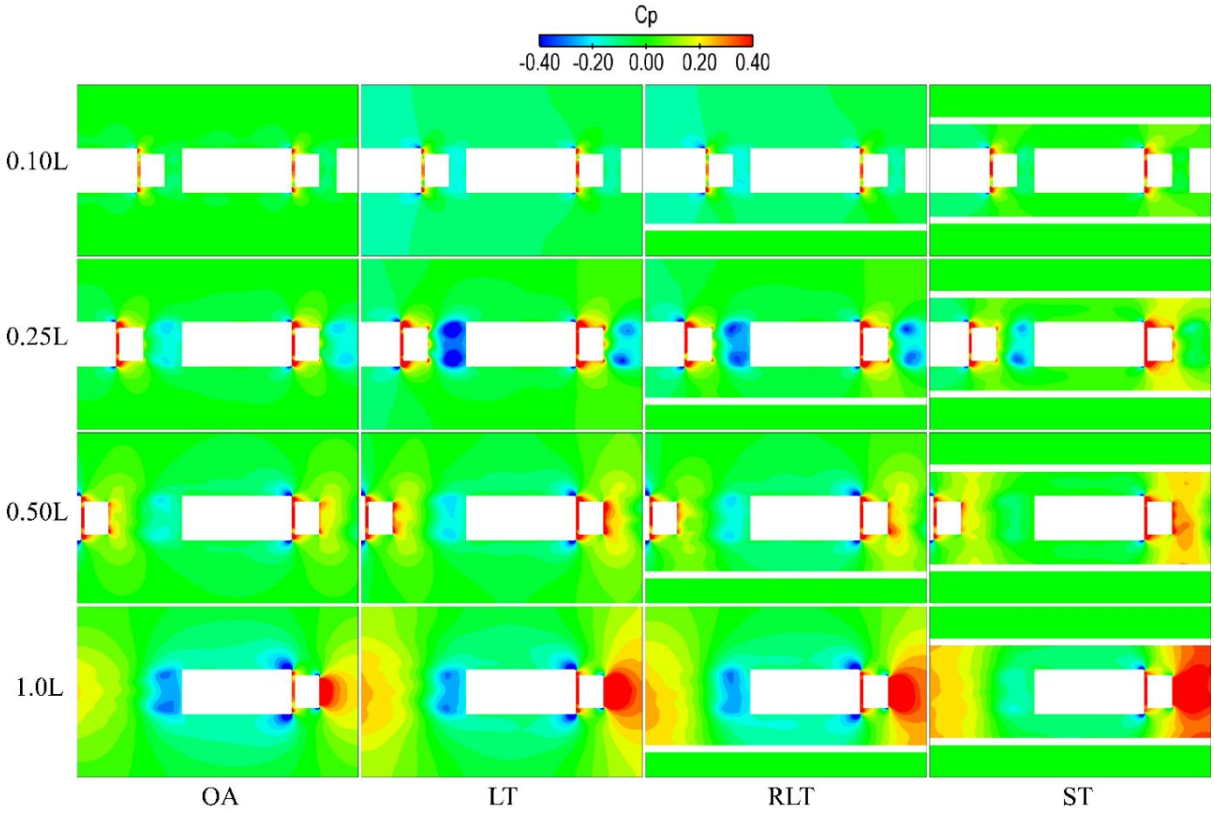

Figure 16. Top view of time-averaged pressure coefficient fields around the fifth lorry in the platoons with different inter-vehicle spacings and running under different circumstances. The data are obtained at the horizontal plane of $z/H = 0.57$. The pressure magnitude is coded by the colour.

To further illustrate how the inter-vehicle spacing affects the airflow in the rear region of the intermediate lorries, Figure 17 compares the time-averaged velocity fields (over the period of $\tau = 7.5 \sim 17.5$) in this region of the fifth lorry for different cases. When the inter-vehicle spacing is larger than 0.25L, there exist two counter-rotating vortices in this region for all the cases. As the inter-vehicle spacing is reduced to 0.25L, the flow structures change dramatically. The bottom vortex is highly compressed and almost disappears when the inter-vehicle spacing is further decreased to 0.1L. The upper vortex also shrinks in size as the inter-vehicle spacing decreases and becomes invisible at the spacing of 0.25L. As a result, the airflow moves directly upward rather than impinging on the cab's front. These changes in flow structures suggest that the frontal pressures for the intermediate lorries decrease with the inter-vehicle spacing.

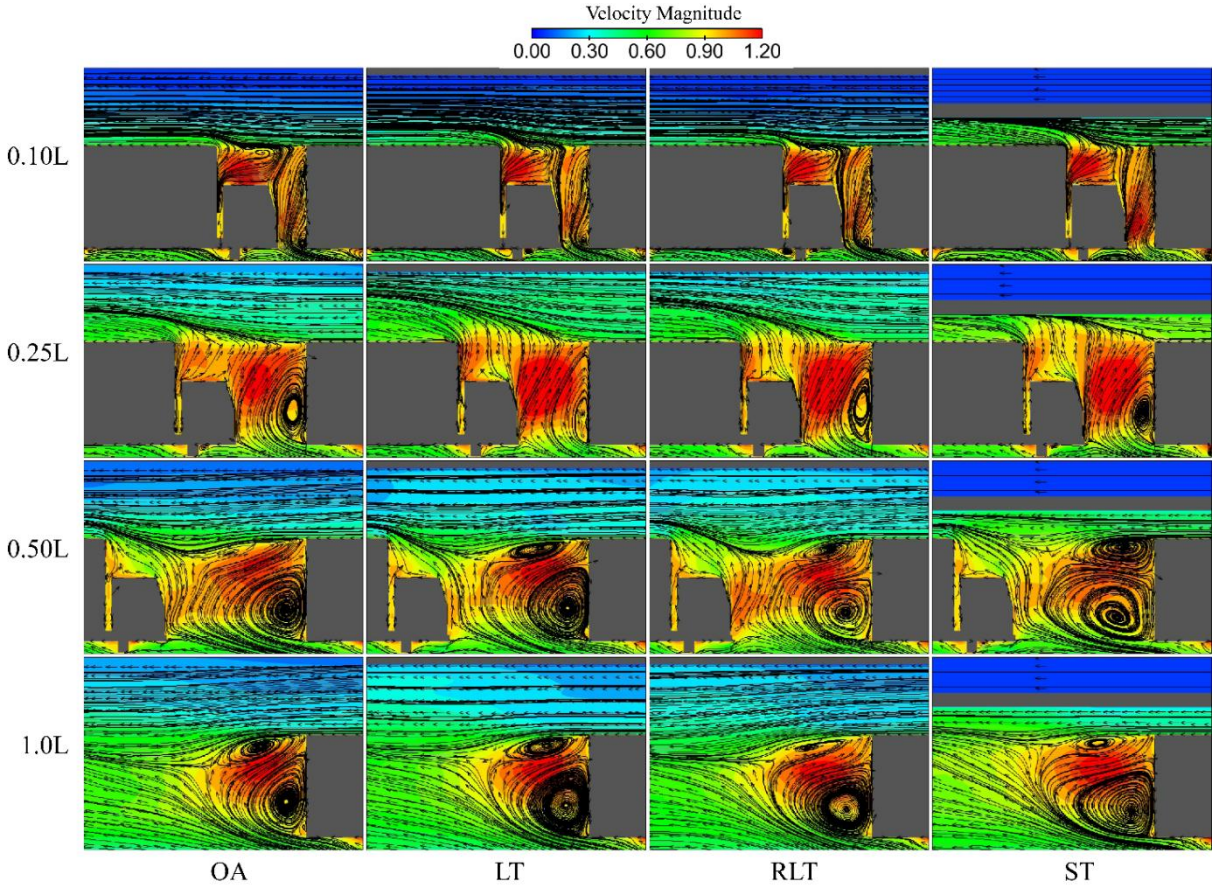

Figure 17. Time-averaged velocity fields in the rear region of the fifth lorry in the platoons with different inter-vehicle spacings and running under different circumstances. The data are obtained at the centreline plane of $y/H=0$. The solid lines are streamlines and the arrows represent velocity vectors. The velocity magnitude is coded by the colour.

4.2.2 *Surface pressure analysis*

Based on the analysis above, the first and the last lorries show expected changes in the flow fields due to platooning, but the behaviours of intermediate lorries are non-trivial. Therefore, the surface pressure analysis in this subsection focuses on the intermediate lorries. Again, the fifth lorry is taken as a representative example.

Figure 18 presents the time-averaged surface coefficients (over the time of τ=7.5~17.5) of the fifth lorries in the platoons with different inter-vehicle spacings and running under different circumstances. The surface pressure drops significantly near the edge of the lorry cab, where the strongest flow separation occurs. These suction peaks are stronger for the RLT cases. Thanks to the more effective shielding at smaller inter-vehicle spacings, the pressure on the cab's front surface decreases for all the cases as the inter-vehicle spacing decreases, with the largest drop occurring between 0.25L and 0.1L. The pressures on the box's top and rear surfaces also decrease with the inter-vehicle spacing in the open air, although to not a greater extent. While in the tunnels, the pressures on the lorry box surfaces do not change monotonically but exhibit anomalous behaviour at the inter-vehicle spacing of 0.25L. Compared to the data for other inter-vehicle spacings, the top surface of the lorry box has a relatively larger value at this spacing, while its rear surface is relatively lower.

The anomaly in the surface pressure for the 0.25L case is also observed along the cross-section of the box (see Figure 19). The data are obtained in the position just behind the flow separation region, so most of the values are negative. The progressively increased pressure coefficients for most of the cases again demonstrate that the shielding effect due to platooning is more efficient at smaller inter-vehicle spacings. However, the data for the 0.25L cases in the tunnels do not follow the monotonic trend. In addition, when the platoon travels along the right lane of the large tunnel, the surface pressures along the box section lose the symmetry slightly, manifesting the effect of the traffic lane.

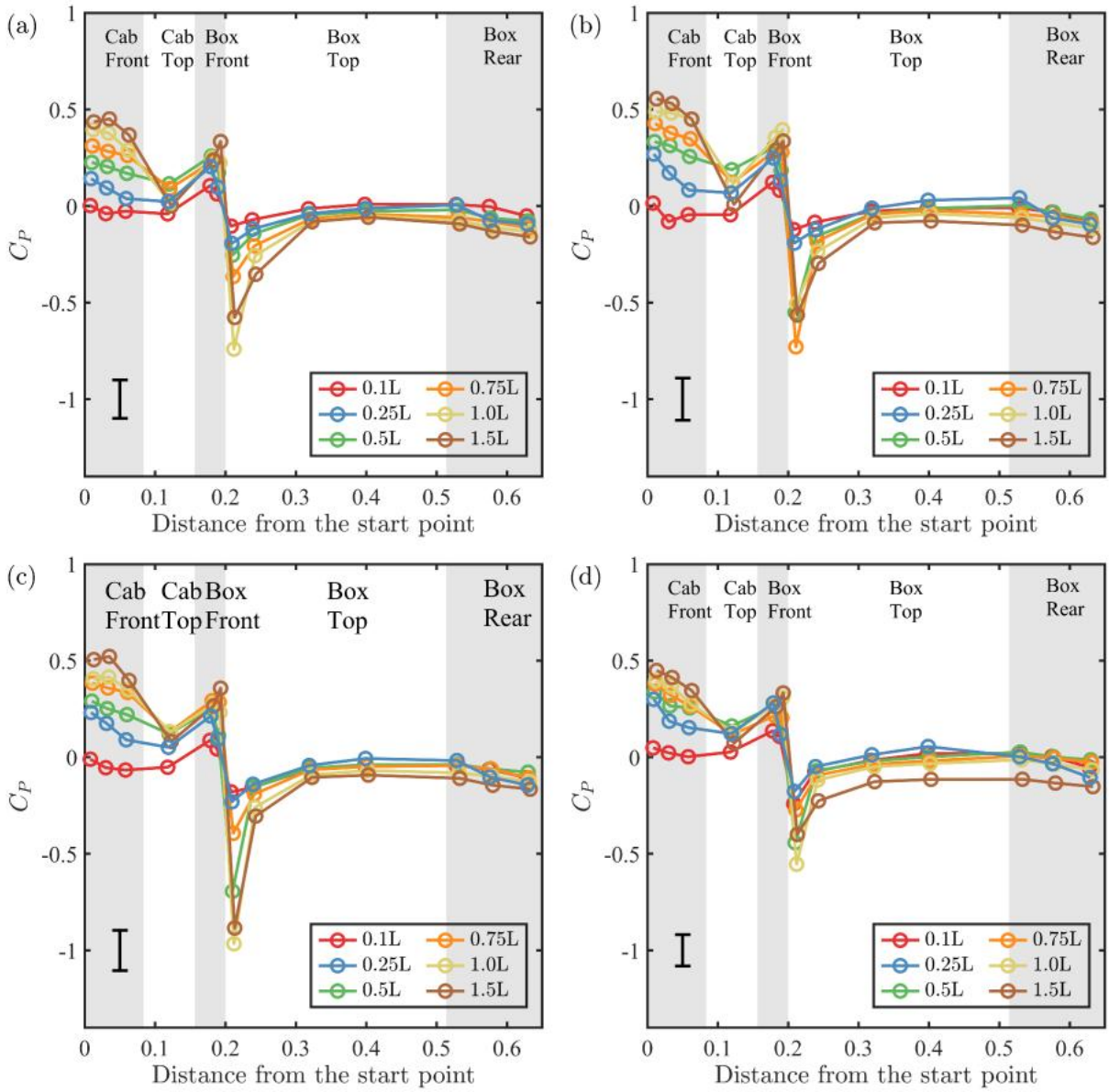

Figure 18. Time-averaged surface pressure coefficients of the fifth lorries in the platoons with different inter-vehicle spacings and running under different circumstances: (a) in the open air, (b) in the large tunnel, (c) along the right traffic lane of the large tunnel and (d) in the small tunnel. The data are obtained along the central line of the lorry (see the solid line O1 in Figure 1) and the error bars indicate the largest r.m.s. values in the simulations. The shaded areas are used to distinguish different regions along the lorry's surface.

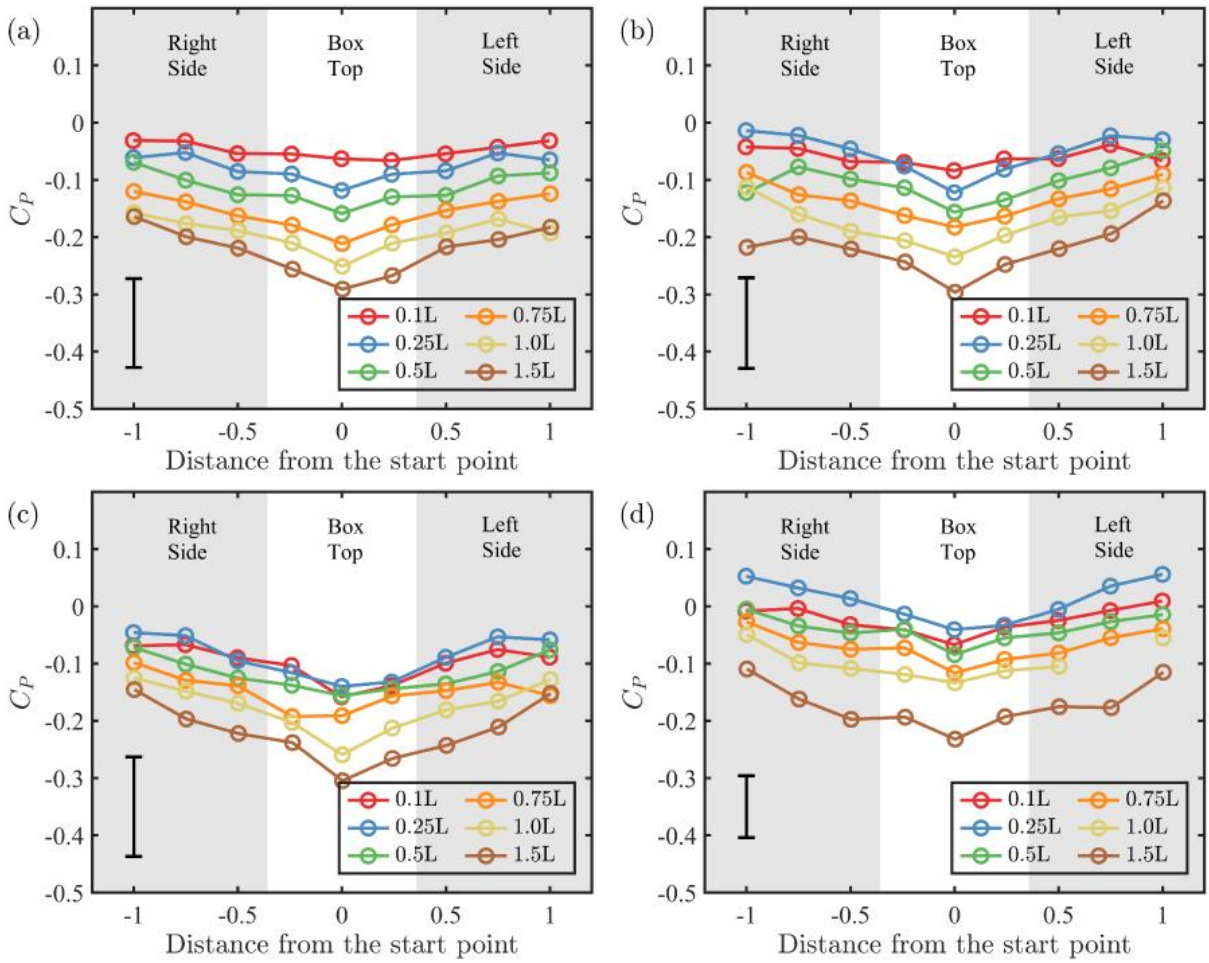

Figure 19. Time-averaged surface pressure coefficients of the fifth lorries in the platoons with different inter-vehicle spacings and running under different circumstances: (a) in the open air, (b) in the large tunnel, (c) along the right traffic lane of the large tunnel and (d) in the small tunnel. The data are obtained along the front loop of the box' cross-section (see the solid line O2 in Figure 1) and the error bars indicate the largest r.m.s. values in the simulations. The shaded areas are used to distinguish different regions along the lorry's box section.

4.2.3 *Drag Force analysis*

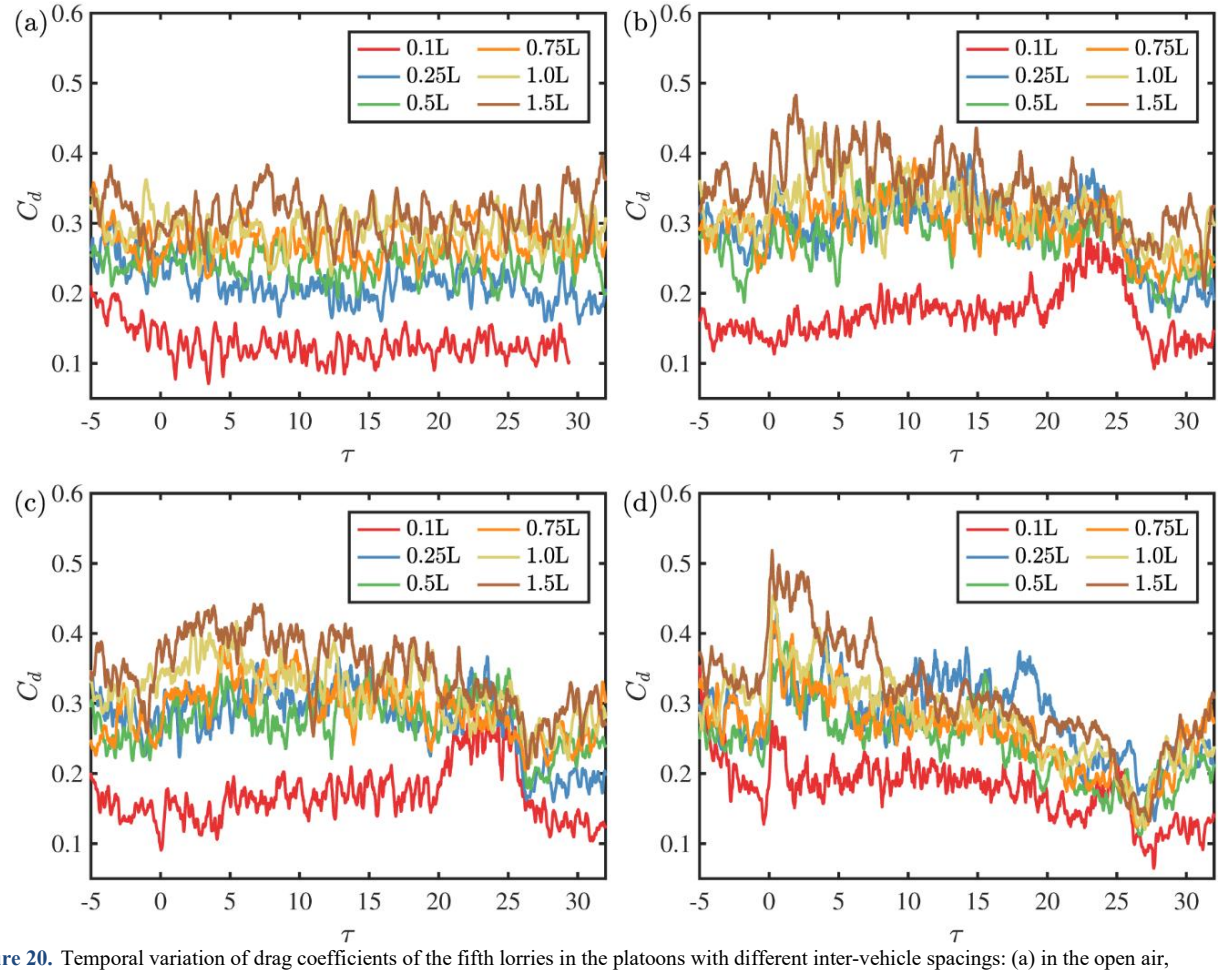

Figure 20. Temporal variation of drag coefficients of the fifth lorries in the platoons with different inter-vehicle spacings: (a) in the open air, (b) in the large tunnel, (c) along the right traffic lane of the large tunnel, and (d) in the small tunnel.

Following the surface pressure analysis, Figure 20 presents the temporal variation of the drag coefficients of the fifth lorries for different cases. Clearly, the shielding effect is most efficient at the inter-vehicle spacing of 0.1L for all the cases. As discussed in Section 4.2.1, the low vortex in the wake region almost disappears at this spacing, and the airflow directly moves upward rather than impinging on the cab's front, which leads to a significant reduction in the frontal surface pressure and thus the drag force. A close look at the data reveals that the drag coefficient in the open air decreases in a monotonic manner with decreasing inter-vehicle spacing. However, owing to the anomaly occurring at the spacing of 0.25L, the drag coefficients in the tunnels do not follow the monotonic trend, regardless of the tunnel size and traffic lane.

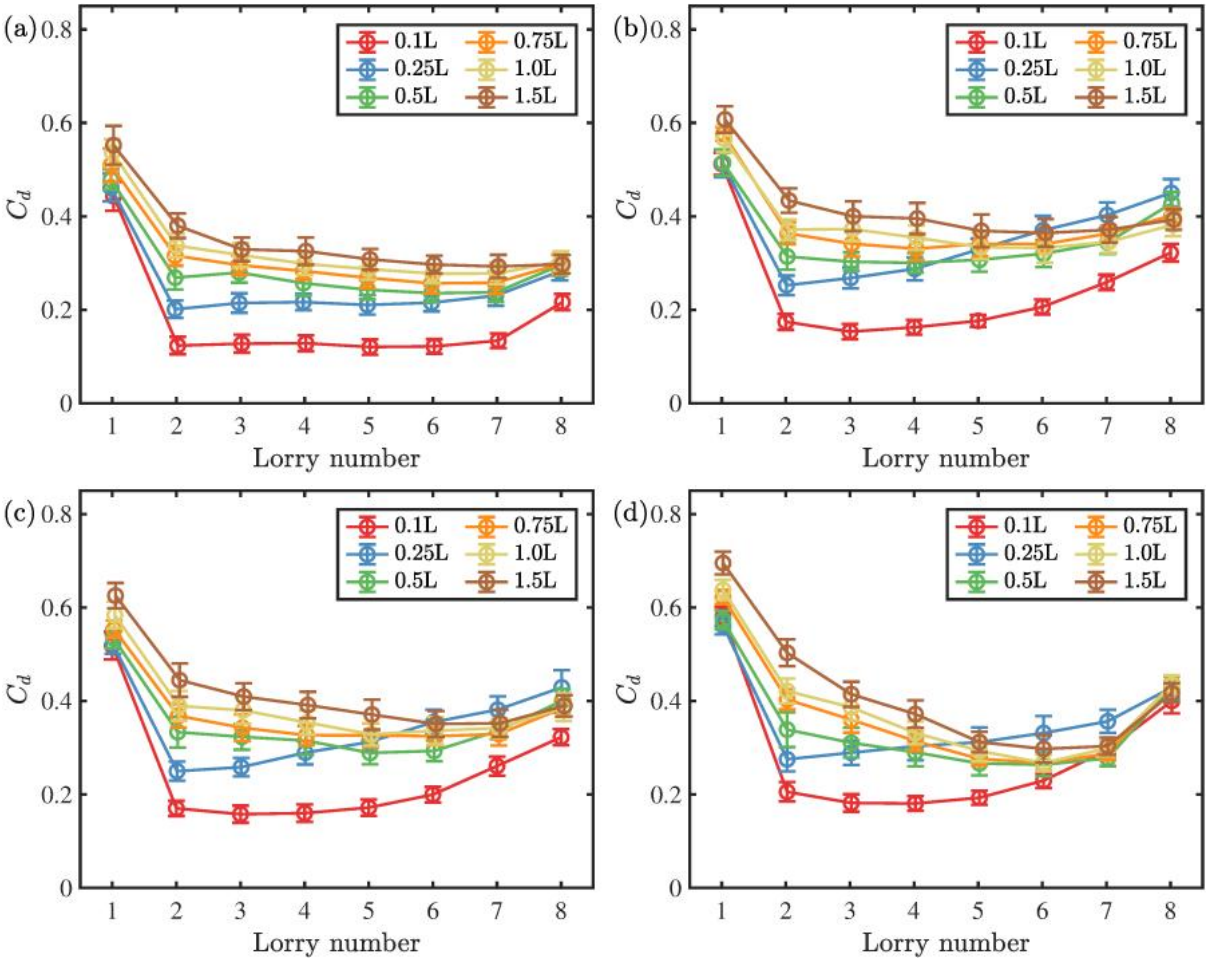

Figure 21. Time-averaged drag coefficients of all lorries in the platoons with different inter-vehicle spacing: (a) in the open air, (b) in the large tunnel, (c) along the right traffic lane of the large tunnel, and (d) in the small tunnel.

To examine the effect of the inter-vehicle spacing quantitatively, Figure 21 compares the time-averaged drag coefficients of all lorries in the platoons with different inter-vehicle spacings. As seen in Figure 21(a), the variation trends of the drag coefficients from the first to the last lorries are similar for different inter-vehicle spacings in the open air. Specifically, the drag coefficients first drop sharply between the leading and the second lorries and then decrease slightly (or remain almost the same) for the following ones. Some exceptions are coming from the last lorries in the platoons with small inter-vehicle spacings, which have stronger negative pressures in the rear regions (as shown in Figure 15) and thus larger drag coefficients. For the platoons running in the tunnels, the situation is a bit complicated. When the inter-vehicle spacing is larger than 0.25L, the variation curves of the drag coefficient in the large tunnel are similar to those in the open air, but the curves in the small tunnel show more significant drag reductions (except for the last lorries). As the inter-vehicle spacing is reduced to 0.25L, the drag coefficients in the tunnels, regardless of the tunnel size and traffic lane, still decrease between the first and the second lorries but increase consistently afterward for the trailing lorries. As a result, some trailing lorries in the tunnels have greater drag coefficients at this spacing than those at larger spacings. With the inter-vehicle spacing further decreasing to 0.1L, the drag-coefficient curves for the first four lorries in the tunnels look like the cases in the open air, but the curves for the last four lorries look like the cases in the tunnels with the spacing of 0.25L.

As the inter-vehicle spacing (as well as the blockage ratio) has different impacts on different lorries in the platoons, it is more meaningful to compare the overall drag coefficient experienced by the whole platoon, which is shown in Figure 22(a). It is seen that the data in the open air increases monotonically with the inter-vehicle spacing, but the increasing rate becomes slower for larger spacings. For the results in the tunnels, their dependences on the inter-vehicle spacing are similar to that in the open air, except for the anomalous behaviour at the inter-vehicle spacing of 0.25L. A somewhat interesting finding in Figure 22(a) is that the overall drag coefficients of the platoons in the small and large tunnels are almost the same. This finding recalls the results shown in Figure 13: compared to the small tunnel, the drag coefficients in the large tunnel are lower for the first two lorries, but they become higher for the fourth to the seventh lorries, thus resulting in the practically equal magnitude of the overall drag coefficients in both tunnels. Similar to the almost identical drag reduction ratios

between the large tunnels and the open air as shown in Figure 13 (b), it is not clear at this stage whether the present finding is valid for other tunnel sizes. More blockage ratios should be explored in the future.

When evaluating the drag reduction ratio defined by $(1-C_d/C_{d-single})\times 100\%$ (see Figure 22(b)), the results become more interesting. First of all, no "drag penalty" is observed in the present study. As mentioned in the introduction, the "drag penalty" phenomenon was mostly reported for short platoons formed by other types of vehicles with small inter-vehicle spacing [13, 18, 32, 33, 36, 37]. For the present platoon formed by eight box-type lorries, considerable drag reduction is found for all the inter-vehicle spacings, with the largest reduction occurring at the inter-vehicle spacing of 0.1L. Secondly, although the platoons in the large tunnel have the same magnitudes of drag coefficients as those in the small tunnel, the drag reduction ratios are almost identical to the cases in the open air, except for the 0.25L spacing. For the inter-vehicle spacing larger than 0.25L, the drag reduction ratios in the small tunnel are about 15% larger than those in the large tunnels and the open air. The differences become relatively small when the inter-vehicle spacing is 0.1L, as the whole platoon largely resembles a single freight train for such a small inter-vehicle spacing.

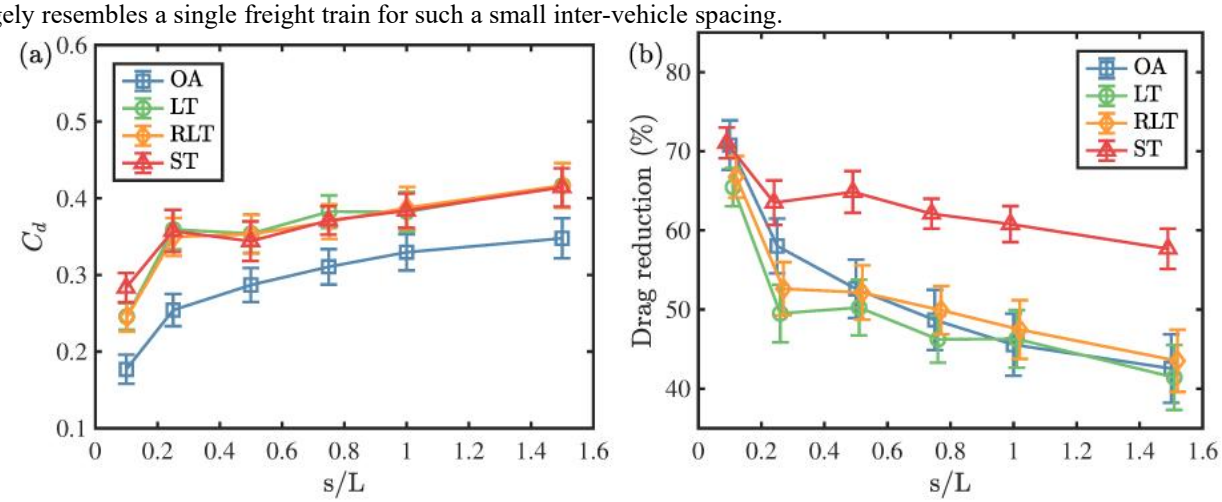

Figure 22. The effect of inter-vehicle spacing on (a) the overall drag coefficients and (b) the overall drag reduction ratio in terms of $(1-C_d/C_{d-single})\times 100\%$ for the whole platoons running under different circumstances. The data are taken from Figure 22 and averaged over all the lorries with the same inter-vehicle spacing and under the same circumstance.

5. Conclusions

This paper presents a numerical study of the aerodynamics associated with lorry platoons travelling through road tunnels. By making a detailed analysis of the slipstream velocity and pressure fields, surface pressures, and aerodynamic forces, the effects of the blockage ratio (i.e., the tunnel size), the traffic lane, and the inter-vehicle spacing of the platoon are investigated. The major findings are summarized as follows.

- As the blockage ratio decreases, the piston effect becomes less effective, so the velocity and pressure fields in the large tunnel are weaker than those in the small tunnel. The drag variations when lorries enter/leave the large tunnel also decrease compared to the data in the small tunnel. On the other hand, the flow structures in the large tunnel are qualitatively similar to those in the open air. As a result, although the lorries running in the large tunnel experience greater drag coefficients than those in the open air, the drag reduction ratios due to platooning are almost the same for these cases. However, it is not clear whether this phenomenon is valid for other tunnel sizes, so more blockage ratios should be explored in the future.
- When the platoon is travelling along the right lane of the large tunnel, the wake structures and the pressure fields become asymmetric. The airflow on the side closer to the tunnel wall becomes stronger, but the effects are not as significant as the influence of the blockage ratio. The drag coefficients as well as the drag reduction ratios are nearly identical to the values when the platoon is travelling along the centerline of the large tunnel.
- The inter-vehicle spacing of the platoon has small effects on the pressure fields around the leading and the last lorries but modifies the pressure differences and the flow structures between the intermediate lorries significantly. When the inter-vehicle spacing is above 0.25L, there are two counter-rotating recirculation vortices in the gap region between intermediate lorries. As the inter-vehicle spacing decreases, the bottom vortex is compressed and the upper vortex becomes less distinguishable. As a result, the airflow moves directly upward rather than impinging on the cab's front, which increases the surface pressures on the box section of the intermediate lorries.

- Due to the substantial shielding effect, the frontal surface pressures of the intermediate lorries decrease dramatically with the inter-vehicle spacing decreasing. However, owing to the influence of the tunnel walls on the flow structures, the intermediate lorries for the 0.25L platoons in the tunnels have higher surface pressures on the lorry's box and lower surface pressures in the rear region. This anomaly in the surface pressure leads to anomalous drag behaviour at this inter-vehicle spacing for the platoons in the tunnels.

Based on the findings above, the strategy to maximize the drag reduction for a lorry platoon in the open air is to reduce its inter-vehicle spacing as much as possible. This strategy is mostly applicable to the lorry platoon running in road tunnels, which is independent of the tunnel size and the traffic lane. However, due to the anomalous drag behaviour at 0.25L, the optimal inter-vehicle spacing for a lorry platoon running in the tunnel should be carefully considered. Moreover, different types of vehicles, especially different frontal geometry, would result in different flow structures and thus induce different drag properties [20, 32]. Therefore, the effect of vehicle geometry is an important issue to explore in the future. In addition, the vehicle number in the platoon would have a potential effect on the drag reduction behaviours [13, 19], so this issue also deserves further study.

Acknowledgments

The authors would like to thank the computational support from the Centre for Computational Science and Engineering at the Southern University of Science and Technology. This work was supported by an EPSRC-funded project entitled 'The aerodynamics of close running ground vehicles – EP/N004213/1', the National Natural Science Foundation of China (Grant No. 11988102), and the Department of Science and Technology of Guangdong Province (Grant No. 2019B21203001).

Conflict of interest

The authors report there are no competing interests to declare.

References

[1] P. Dabnichki, E. Avital. Influence of the postion of crew members on aerodynamics performance of two-man bobsleigh. *Journal of Biomechanics*. 2006; 39(15): 2733–2742. https://doi.org/10.1016/j.jbiomech.2005.10.011.

[2] B. Blocken, Y. Toparlar, T. van Druenen, T. Andrianne. Aerodynamic drag in cycling team time trials. *Journal of Wind Engineering and Industrial Aerodynamics*. 2018; 182: 128–145. https://doi.org/10.1016/j.jweia.2018.09.015.

[3] B. Blocken, Y. Toparlar, T. Andrianne. Aerodynamic benefit for a cyclist by a following motorcycle. *Journal of Wind Engineering and Industrial Aerodynamics*. 2016; 155: 1–10. https://doi.org/10.1016/j.jweia.2016.04.008.

[4] C. Beves, S. *Ferguson. Analysing the aerodynamics of the fastest ever marathon.* https://www.theengineer.co.uk/content/in-depth/analysing-the-aerodynamics-of-the-fastest-ever-marathon [Accessed 1 July 2021].

[5] J. Katz. Aerodynamics of race cars. *Annual Review of Fluid Mechanics*, 2006; 38: 27–63. https://doi.org/10.1146/annurev.fluid.38.050304.092016.

[6] A. Mirzaeinia, F. Heppner, M. Hassanalian. An analytical study on leader and follower switching in V-shaped Canada goose flocks for energy management purposes. *Swarm Intelligence*. 2020; 14: 117–141. https://doi.org/10.1007/s11721-020-00179-x.

[7] T. Morel, M. Bohn. Flow over two circular disks in tandem. *Journal of Fluids Engineering*. 1980; 102: 104–111. https://doi.org/10.1115/1.3240599.

[8] L. Ljungkrona, B. Sundén. Flow visualization and surface pressure measurement on two tubes in an inline arrangement. *Experimental Thermal and Fluid Science*. 1993; 6: 15–27. https://doi.org/10.1016/0894-1777(93)90037-J.

[9] N. Kondo, D. Matsukuma. Numerical simulation for flow around two circular cylinders in tandem. *International Journal of Computational Fluid Dynamics*. 2005; 19: 277–288. https://doi.org/10.1080/10618560500234345.

[10] H. Hirano, A. Maruoka, M. Ikenouchi. Numerical fluid flow analysis for aerodynamic response characteristics of tandem circular cylinders. *International Journal of Computational Fluid Dynamics*. 1998; 9: 197–208. https://doi.org/10.1080/10618569808940852.

[11] M. Bull, A. Blazewicz, J. Pickles, D. Bies. Interaction between a vortex wake and an immersed rectangular plate. *Experimental Thermal and Fluid Science*. 1996; 12: 209–220. https://doi.org/10.1016/0894-1777(95)00099-2.

[12] K. Koenig, A. Roshko. An experimental study of geometrical effects on the drag and flow field of two bluff bodies separated by a gap. *Journal of Fluid Mechanics*. 1985; 156: 167-204. https://doi.org/10.1017/S002211208500204X.

[13] G. Le Good, M. Resnick, P. Boardman, B. Clough. Effects on the aerodynamic characteristics of vehicles in longitudinal proximity due to changes in style. *2nd CO2 Reduction for Transportation Systems Conference*. Turin, Italy: SAE Technical Papers; 2018. p.1-15. https://doi.org/10.4271/2018-37-0018.

[14] B. R. McAuliffe, M. Ahmadi-Baloutaki. A wind-tunnel investigation of the influence of separation distance, lateral stagger, and trailer configuration on the drag-reduction potential of a two-truck platoon. *SAE International Journal of Commercial Vehicles*. 2018; 11(2): 125-150. https://doi.org/10.4271/02-11-02-0011.

[15] F. H. Robertson, F. Bourriez, M. He, D. Soper, C. Baker, H. Hemida, M. Sterling. An experimental investigation of the aerodynamic flows created by lorries travelling in a long platoon. *Journal of Wind Engineering and Industrial Aerodynamics*. 2019; 193: 103966. https://doi.org/10.1016/j.jweia.2019.103966.

[16] K. Salari, J. Ortega. Experimental investigation of the aerodynamic benefits of truck platooning. *WCX World Congress Experience*. Washington, The United States: *SAE Technical Papers*; 2018. https://doi.org/10.4271/2018-01-0732.

[17] L. Tsuei, Ö. Savaş. Transient aerodynamics of vehicle platoons during in-line oscillations. *Journal of Wind Engineering and Industrial Aerodynamics*. 2001; 89: 1085–1111. https://doi.org/10.1016/S0167-6105(01)00073-3.

[18] M. Zabat, N. Stabile, S. Farascaroli, F. Browand. *The aerodynamic performance of platoons: A Final Report*. California Partners for Advanced Transportation Technology. 1995. https://escholarship.org/uc/item/8ph187fw.

[19] G. Le Good, P. Boardman, M. Resnick, B. Clough. An investigation of aerodynamic characteristics of three bluff bodies in close longitudinal proximity. *WCX SAE World Congress Experience*. Washington, The United States: SAE International; 2019. https://doi.org/10.4271/2019-01-0659.

[20] B. McAuliffe, M. Ahmadi-Baloutaki. An investigation of the influence of close-proximity traffic on the aerodynamic drag experienced by tractor-trailer combinations. *SAE Technical Papers*. 2019; 1(3): 1251-1264. https://doi.org/10.4271/2019-01-0648.

[21] J. Törnell, S. Sebben, P. Elofsson. Experimental investigation of a two-truck platoon considering inter-vehicle distance, lateral offset and yaw. *Journal of Wind Engineering and Industrial Aerodynamics*. 2021; 213: 104596. https://doi.org/10.1016/j.jweia.2021.104596.

[22] C. Bonnet, H. Fritz. Fuel consumption reduction in a platoon: Experimental results with two electronically coupled trucks at close spacing. *SAE Technical Papers*. 2000; 2000-01-3056. https://doi.org/10.4271/2000-01-3056.

[23] M.P. Lammert, A. Duran, J. Diez, K. Burton, A. Nicholson. Effect of platooning on fuel consumption of class 8 vehicles over a range of speeds, following distances, and mass. *SAE 2014 Commercial Vehicle Engineering Congress (COMVEC).* Rosemont, United States: SAE International Journal of Commercial Vehicles; 2014. https://doi.org/10.4271/2014-01-2438.

[24] H. Humphreys, D. Bevly. Computational fluid dynamic analysis of a generic 2 truck platoon. *SAE 2016 Commercial Vehicle Engineering Congress.* Rosemont, United States: SAE Technical Papers; 2016. https://doi.org/10.4271/2016-01-8008.

[25] R. Veldhuizen, G.M.R. Van Raemdonck, J.P. Van der Krieke. Fuel economy improvement by means of two European tractor semi-trailer combinations in a platooning formation. *Journal of Wind Engineering and Industrial Aerodynamics*. 2019; 188: 217–234. https://doi.org/10.1016/j.jweia.2019.03.002.

[26] F. Browand, J. Mcarthur, C. Radovich. *Fuel saving achieved in the field test of two tandem trucks.* UC Berkeley: California Partners for Advanced Transportation Technology. 2004. https://escholarship.org/uc/item/29v570mm.

[27] B. McAuliffe, M. Croken, M. Ahmadi-Baloutaki, A. Raeesi. *Fuel-economy testing of a three-vehicle truck platooning system.* UC Berkeley: California Partners for Advanced Transportation Technology. 2017. https://escholarship.org/uc/item/7g37w4fb.

[28] M. He, S. Huo, H. Hemida, F. Bourriez, F. H. Robertson, D. Soper, M. Sterling, C. Baker. Detached eddy simulation of a closely running lorry platoon. *Journal of Wind Engineering and Industrial Aerodynamics*. 2019; 193: 103956. https://doi.org/10.1016/j.jweia.2019.103956.

[29] A. Davila, E. Aramburu, A. Freixas. Making the best out of aerodynamics: Platoons. *SAE 2013 World Congress & Exhibition.* Michigan, the United States: SAE Technical Papers; 2013. https://doi.org/10.4271/2013-01-0767.

[30] C.H. Bruneau, K. Khadra, I. Mortazavi. Flow analysis of square-back simplified vehicles in platoon. *International Journal of Heat and Fluid Flow*. 2017; 66: 43–59. https://doi.org/10.1016/j.ijheatfluidflow.2017.05.008.

[31] M. Hammache, M. Michaelian, F. Browand. Aerodynamic forces on truck models, including two trucks in tandem. *SAE 2002 World Congress*. Michigan, the United States: SAE Technical Paper; 2002. https://doi.org/10.4271/2002-01-0530.

[32] H. Ebrahim, R. Dominy. Wake and surface pressure analysis of vehicles in platoon. *Journal of Wind Engineering and Industrial Aerodynamics*. 2020; 201: 104144. https://doi.org/10.1016/j.jweia.2020.104144.

[33] M. Mirzaei, S. Krajnović. Large eddy simulations of flow around two generic vehicles in a platoon. In: A. Segalini. (ed.). *Proceedings of the 5th International Conference on Jets, Wakes Separated Flows (ICJWSF2015)*. Stockholm, Sweden: Springer Proceedings in Physics; 2016. p.283–288. https://doi.org/10.1007/978-3-319-30602-5_35.

[34] P. Schito, F. Braghin. Numerical and experimental investigation on vehicles in platoon. *SAE International Journal of Commercial Vehicles*. 2012; 5(1): 63-71. https://doi.org/10.4271/2012-01-0175.

[35] European Commission. *Safe road trains for the environment; developing strategies and technologies to allow vehicle platoons to operate on normal public highways with significant environmental, safety and comfort benefits*. https://cordis.europa.eu/project/rcn/92577/factsheet/en. [Accessed 1 january 2023]

[36] R.M. Pagliarella, S. Watkins, A. Tempia. Aerodynamic performance of vehicles in platoons: The influence of backlight angles. *SAE World Congress & Exhibition*. Michigan, the United States: SAE Technical Papers; 2007. https://doi.org/10.4271/2007-01-1547.

[37] S. Watkins, G. Vino. The effect of vehicle spacing on the aerodynamics of a representative car shape. *Journal of Wind Engineering and Industrial Aerodynamics*. 2008; 96(6-7): 1232–1239. https://doi.org/10.1016/j.jweia.2007.06.042.

[38] T. Gheyssens, G. Van Raemdonck. Effect of the frontal edge radius in a platoon of bluff bodies. *SAE International Journal of Commercial Vehicles*. 2016; 9(2): 371-380. https://doi.org/10.4271/2016-01-8149.

[39] J. Törnell, S. Sebben, D. Söderblom. Influence of inter-vehicle distance on the aerodynamics of a two-truck platoon. *International Journal of Automotive Technology*. 2021; 22: 747–760. https://doi.org/10.1007/s12239-021-0068-5.

[40] T.Y. Chen, Y.T. Lee, C.C. Hsu. Investigations of piston-effect and jet fan-effect in model vehicle tunnels. *Journal of Wind Engineering and Industrial Aerodynamics*. 1998; 73: 99–110. https://doi.org/10.1016/S0167-6105(97)00281-X.

[41] M. Sambolek. Model testing of road tunnel ventilation in normal traffic conditions. *Engineering Structures*, 2004; 26: 1705–1711. https://doi.org/10.1016/j.engstruct.2004.06.001.

[42] J. Katolický, M. Jícha. Eulerian–Lagrangian model for traffic dynamics and its impact on operational ventilation of road tunnels. *Journal of Wind Engineering and Industrial Aerodynamics*. 2005; 93: 61–77. https://doi.org/10.1016/j.jweia.2004.09.002.

[43] S. Lee, Y. Park, J. Kim. An evaluation of factors influencing drag coefficient in double-deck tunnels by CFD simulations using factorial design method. *Journal of Wind Engineering and Industrial Aerodynamics*. 2018; 180: 156–167. https://doi.org/10.1016/j.jweia.2018.07.018.

[44] K. Ashrafi, M. Shafie-pour, M. Kalhor, V. Esfahanian. Numerical simulation of air pollutant distribution in urban tunnels. *Environ Model Assess*. 2012; 17: 555–564. https://doi.org/10.1007/s10666-012-9308-4.

[45] U. Bhautmage, S. Gokhale. Effects of moving-vehicle wakes on pollutant dispersion inside a highway road tunnel. *Environmental Pollution*. 2016; 218: 783–793. https://doi.org/10.1016/j.envpol.2016.08.002.

[46] F. Wang, M. Wang, Q. Wang, D. Zhao. An improved model of traffic force based on CFD in a curved tunnel. *Tunnelling and Underground Space Technology*. 2014; 41: 120–126. https://doi.org/10.1016/j.tust.2013.12.006.

[47] F. Wang, M. Wang, S. He, Y. Deng. Computational study of effects of traffic force on the ventilation in highway curved tunnels. *Tunnelling and Underground Space Technology*. 2011; 26: 481–489. https://doi.org/10.1016/j.tust.2011.01.003.

[48] X. Song, Y. Zhao. Numerical investigation of airflow patterns and pollutant dispersions induced by a fleet of vehicles inside road tunnels using dynamic mesh Part II: Pollutant dispersion and exposure levels. *Atmospheric Environment*. 2019; 210: 198–210. https://doi.org/10.1016/j.atmosenv.2019.04.028.

[49] J. Sike, G. Yanfeng, Z. Guangli. Flow field development and energy evolution in road tunnels with unidirectional uniform traffic. *Journal of Wind Engineering and Industrial Aerodynamics*. 2015; 147: 66–76. https://doi.org/10.1016/j.jweia.2015.09.011.

[50] X. Zhang, F.H. Robertson, D. Soper, H. Hemida, S.D. Huang. Investigation of the aerodynamic phenomena associated with a long lorry platoon running through a tunnel. *Journal of Wind Engineering and Industrial Aerodynamics*. 2021; 210: 104514. https://doi.org/10.1016/j.jweia.2020.104514.

[51] F. Cheli, R. Corradi, E. Sabbioni, G. Tomasini. Wind tunnel tests on heavy road vehicles: Cross wind induced loads—Part 1. *Journal of Wind Engineering and Industrial Aerodynamics*. 2011; 99: 1000–1010. https://doi.org/10.1016/j.jweia.2011.07.009.

[52] N. Patel, M. He, H. Hemida, A. Quinn. Large-eddy simulation of the airflow around a truck. *Journal of Wind Engineering and Industrial Aerodynamics*. 2019; 195: 104017. https://doi.org/10.1016/j.jweia.2019.104017.

[53] A.D. Quinn, M. Sterling, A.P. Robertson, C.J. Baker. An investigation of the wind-induced rolling moment on a commercial vehicle in the atmospheric boundary layer. *Proceedings of the Institution of Mechanical Engineers, Part D: Journal of Automobile Engineering*. 2007; 221: 1367–1379. https://doi.org/10.1243/09544070JAUTO537.

[54] F.H. Robertson, D. Soper, C. Baker. Unsteady aerodynamic forces on long lorry platoons. *Journal of Wind Engineering and Industrial Aerodynamics*. 2021; 209: 104481. https://doi.org/10.1016/j.jweia.2020.104481.

[55] C.J. Baker, S.J. Dalley, T. Johnson, A. Quinn, N.G. Wright. The slipstream and wake of a high-speed train. *Proceedings of the Institution of Mechanical Engineers, Part F: Journal of Rail and Rapid Transit*. 2001; 215: 83–99. https://doi.org/10.1243/0954409011531422.

[56] F. Dorigatti, M. Sterling, C.J. Baker, A.D. Quinn. Crosswind effects on the stability of a model passenger train—A comparison of static and moving experiments. *Journal of Wind Engineering and Industrial Aerodynamics*. 2015; 138: 36–51. https://doi.org/10.1016/j.jweia.2014.11.009.

[57] European Normative. Railway applications-aerodynamics-Part4: requirements and test procedures for aerodynamics on open track. *National Standards Authority of Ireland*. 14067-4:2013+A1. 2018. https://infostore.saiglobal.com/preview/is/en/2013/i.s.en14067-4-2013.pdf?sku=1694040

[58] P. Hong, B. Marcu, F. Browand, A. Tucker. Drag forces experienced by two, full-scale vehicles at close spacing. *SAE Technical Papers*. 1998, 980396. https://doi.org/10.4271/980396.

[59] M. Gallagher, J. Morden, C. Baker, D. Soper, A. Quinn, H. Hemida, M. Sterling. Trains in crosswinds – Comparison of full-scale on-train measurements, physical model tests and CFD calculations. *Journal of Wind Engineering and Industrial Aerodynamics*. 2018; 175: 428–444. https://doi.org/10.1016/j.jweia.2018.03.002.

[60] U. Piomelli. Wall-layer models for large-eddy simulations. *Progress in Aerospace Sciences*. 2008; 44: 437–446. https://doi.org/10.1016/j.paerosci.2008.06.001.

[61] J. Dong, Y. Tao, Y. Xiao, J. Tu. Numerical simulation of pollutant dispersion in urban roadway tunnels. *The Journal of Computational Multiphase Flows*. 2017; 9: 26–31. https://doi.org/10.1177/1757482X17694041.

[62] L. Li, G.S. Du, Y.W. Li, Z.G. Liu. Numerical simulation of the transient aerodynamic phenomena associated with a van running into a road tunnel. *2009 Asia-Pacific Power and Energy Engineering Conference*. Wuhan, China: IEEE; 2009. pp.1–4. https://doi.org/10.1109/APPEEC.2009.4918542.

[63] P. Ridley. Modelling pollution dynamics of longitudinally ventilated road tunnels. *Journal of Wind Engineering and Industrial Aerodynamics*. 2017; 163: 55–64. https://doi.org/10.1016/j.jweia.2016.12.003.

[64] G. Chen, X.F. Liang, Li X., Zhou D., Lien F., Wang J.. Dynamic analysis of the effect of platoon configuration on train aerodynamic performance. *Journal of Wind Engineering and Industrial Aerodynamics*. 2021; 211: 104564. https://doi.org/10.1016/j.jweia.2021.104564.

[65] J. Niu, Y. Wang, L. Zhang, Y. Yuan. Numerical analysis of aerodynamic characteristics of high-speed train with different train nose lengths. *International Journal of Heat and Mass Transfer*. 2018; 127: 188–99. https://doi.org/10.1016/j.ijheatmasstransfer.2018.08.041.

[66] M.L. Shur, P.R. Spalart, M.K. Strelets, A.K. Travin. A hybrid RANS-LES approach with delayed-DES and wall-modelled LES capabilities. *International Journal of Heat and Fluid Flow*. 2008; 29: 1638–49. https://doi.org/10.1016/j.ijheatfluidflow.2008.07.001.

[67] M.S. Gritskevich, A.V. Garbaruk, J. Schütze, F.R. Menter. Development of DDES and IDDES Formulations for the k-ω Shear Stress Transport Model. *Flow, Turbulence and Combustion*. 2012; 88: 431–449. https://doi.org/10.1007/s10494-011-9378-4.

[68] H. Hemida, S. Krajnović. Transient simulation of the aerodynamic response of a double-deck bus in gusty winds. *Journal of Fluids Engineering*. 2009; 131: 0311011–03110110. https://doi.org/10.1115/1.3054288.

[69] J. Niu, D. Zhou, T. Liu, X. Liang. Numerical simulation of aerodynamic performance of a couple multiple units high-speed train. *Vehicle System Dynamics*. 2017; 55: 681–703. https://doi.org/10.1080/00423114.2016.1277769.

[70] Z. Chen, T. Liu, X. Zhou, J. Niu. Impact of ambient wind on aerodynamic performance when two trains intersect inside a tunnel. *Journal of Wind Engineering and Industrial Aerodynamics*. 2017; 169: 139–55. https://doi.org/10.1016/j.jweia.2017.07.018.

[71] A. Khayrullina, B. Blocken, W. Janssen, J. Straathof. CFD simulation of train aerodynamics: Train-induced wind conditions at an underground railroad passenger platform. *Journal of Wind Engineering and Industrial Aerodynamics*. 2015; 139: 100–10. https://doi.org/10.1016/j.jweia.2015.01.019.

[72] Y. Liu, H. Hemida, Z. Liu. Large eddy simulation of the flow around a train passing a stationary freight wagon. *Proceedings of the Institution of Mechanical Engineers, Part F: Journal of Rail and Rapid Transit*. 2014; 228: 535–545. https://doi.org/10.1177/0954409713488096.

[73] C.R. Chu, S.Y. Chien, C.Y. Wang, T.R. Wu. Numerical simulation of two trains intersecting in a tunnel. *Tunnelling and Underground Space Technology*. 2014; 42: 161–174. https://doi.org/10.1016/j.tust.2014.02.013.

[74] R. Yoshie, A. Mochida, Y. Tominaga, H. Kataoka, K. Harimoto, T. Nozu, T. Shirasawa. Cooperative project for CFD prediction of pedestrian wind environment in the Architectural Institute of Japan. *Journal of Wind Engineering and Industrial Aerodynamics*. 2007; 95: 1551–1578. https://doi.org/10.1016/j.jweia.2007.02.023.

[75] S. Meng, X. Li, G. Chen, D. Zhou, Z. Chen, S. Krajnovic. Numerical simulation of slipstreams and wake flows of trains with different nose lengths passing through a tunnel. *Tunnelling and Underground Space Technology*. 2021; 108: 103701. https://doi.org/10.1016/j.tust.2020.103701.

[76] S. Wang, J.R. Bell, D. Burton, A.H. Herbst, J. Sheridan, M.C. Thompson. The performance of different turbulence models (URANS, SAS and DES) for predicting high-speed train slipstream. *Journal of Wind Engineering and Industrial Aerodynamics*. 2017; 165: 46–57. https://doi.org/10.1016/j.jweia.2017.03.001.

[77] C. Xia, X. Shan, Z. Yang. Detached-eddy simulation of ground effect on the wake of a high-speed train. *Journal of Fluids Engineering*. 2017; 139: 051101. https://doi.org/10.1115/1.4035804.

[78] D. Flynn, H. Hemida, D. Soper, C. Baker. Detached-eddy simulation of the slipstream of an operational freight train. *Journal of Wind Engineering and Industrial Aerodynamics*. 2014; 132: 1–12. https://doi.org/10.1016/j.jweia.2014.06.016.

[79] X. Zhang. *The aerodynamics of long lorry platoon in a tunnel.* PhD Thesis. University of Birmingham. Ph.D. 2022.